Pergamon

Geochimica et Cosmochimica Acta, Vol. 65, No. 21, pp. 4019–4041, 2001

0016-7037/01 $20.00 + .00

PII S0016-7037(00)00727-X

Glass transition, structural relaxation, and theories of viscosity: A molecular dynamics study of amorphous $CaAl_2Si_2O_8$

NEIL A. MORGAN and FRANK J. SPERA

Institute for Crustal Studies and Department of Geological Sciences, 2118 Webb Hall, University of California, Santa Barbara, CA 93106, USA

(*Received September* 26, 2000; *accepted in revised form June* 7, 2001)

Abstract—Molecular dynamics (MD) simulation provides a unique window into the dynamics of amorphous silicates of geochemical importance. Of special interest are theories of the glass transition and viscosity when an equilibrium liquid passes through the metastable supercooled liquid state to become a nonequilibrium glass. Viscosity increases enormously in a small temperature range around the glass transition temperature. Twenty MD simulations utilizing 1300 particles were conducted for $CaAl_2Si_2O_8$ at temperatures in the range 1700 to 5000 K along the ~ 1 GPa isobar. A pairwise potential with Coulombic and Born-Mayer interaction was used in the evaluation of forces. Simulation durations range from 50 to 150 ps. Previously, structures, thermodynamic properties, and tracer diffusivities were determined as a function of temperature for liquid and glass (Morgan and Spera, 2001). Here, the focus is upon atomic cooperative motion at the nanometer scale and theories of viscosity illuminated by correlation analysis and tagged particle dynamics. Dramatic differences in the dynamics of particles monitored by the nongaussian component of atom self-diffusivity, the van Hove correlation function and the intermediate scattering function appear near the (computer) glass transition temperature T_g = 2800 K. At $T < T_g$, the van Hove correlation function for oxygen and calcium exhibits a double-peaked structure characteristic of hopping diffusion through correlated jumps involving neighboring particles to nearest neighbor sites in an otherwise "frozen" structure. The crossover between continuous (hydrodynamic-like) motion and hopping motion shows up in the time dependence of the mean square displacement as a function of temperature and in the temporal decay of microscopic density fluctuations given by the intermediate scattering function. A particle and its neighbors remain trapped for a finite waiting time before undergoing a cooperative thermally activated rearrangement that is based on an elementary hop. The waiting time distribution is strongly temperature dependent and related to the dramatic increase in structural relaxation time as temperature approaches T_g. Three models for the glass transition—the Adam-Gibbs configurational entropy model, mode-coupling theory, and the stochastic trapping diffusion model—are discussed in light of the MD simulations. Although each model offers novel insight into the glass transition and the relationship between structural relaxation and atomic-scale dynamics, no single model is complete. The MD simulations are consistent with a picture of "dynamic heterogeneity" as the cause of the sluggish dynamics as an equilibrium liquid becomes deeply supercooled. At some temperature above the Kauzmann temperature (T_K) where the extrapolated entropy of supercooled liquid equals that of crystalline solid, long-lived, highly cooperative, collective particle motions take place in restricted regions of three-dimensional space. Subsets of particles exhibit faster or slower than average relaxation rates. The relationship of dynamic heterogeneity viewed in three-dimensional Euclidean space to its analog in 6N-dimensional-phase space remains to be elucidated. Specifically, the lifetime and sizes of cooperatively rearranging regions as a function of temperature needs further study. Self-organization of cooperatively rearranging regions demands further investigation as well. *Copyright © 2001 Elsevier Science Ltd*

1. INTRODUCTION

Glasses constitute an important class of materials from both fundamental and practical viewpoints. Although they are among the most ancient natural materials used by humans, knowledge of their structure, dynamics, and properties remains surprisingly incomplete. Unlike crystalline solids and dilute gasses, a reasonably complete theory of liquids and of amorphous (glassy) solids is not available. Glasses are especially important geological materials. On Earth, rapid cooling of magma produces about a billion cubic meters (1 km^3) of glass each year, mainly along the 70,000-km globe-encircling oceanic ridge system. Global geochemical interchange between hydrosphere, biosphere, and lithosphere is strongly influenced by reactions of natural glass with aqueous solutions of varying temperature, pressure, and composition. Glass is also an important material on other planetary bodies. Glass forms during the ubiquitous process of shock compression accompanying hypervelocity impact of planetary materials. An understanding of the nature of glasses, and supercooled and equilibrium liquids is important for a variety of environmental, geoscience, and technological problems.

The literature on glasses, structural relaxation, the glass transition, theories of liquid viscosity, and the connection between the properties and structure of liquids and glasses is vast, reflecting the importance of these problems. Many excellent reviews are available, including those by Zallen (1983), Hansen and McDonald (1986), Zarzycki (1991), Binder (1995), Kob (1995, 1999), Debenedetti (1996), and Angell (1991). The review volume edited by Stebbins et al. (1995) presents a summary of the structure, dynamics, and properties of melts, metastable liquids, and glasses of geochemical importance.

* Author to whom correspondence should be addressed (spera@geol.ucsb.edu).

In this work, the microscopic dynamics of $CaAl_2Si_2O_8$ are studied as a function of temperature from 1700 to 5000 K along the ~ 1 GPa isobar by use of the molecular dynamics (MD) technique. Although cooling through the glass transition is accompanied by little static structural change (Morgan and Spera, 2001), dramatic changes in atom mobility, the rate of structural relaxation, and the qualitative features of atomic-scale motion take place as the glass transition temperature is approached. These changes are elucidated by studying the correlated motions of oxygen, calcium, aluminum, and silicon in stoichiometric $CaAl_2Si_2O_8$ by means of the van Hove correlation function, the intermediate scattering function and the nongaussian part of self-diffusivity. In addition, three existent theories of the glass transition, the Adam-Gibbs configurational entropy model (AGSC), the mode-coupling theory (MCT), and the stochastic trap diffusion model (STDM) are reviewed in light of the MD results.

Several MD studies on liquid and glassy anorthite have been reported previously. These are briefly reviewed to provide a context for the results and conclusions drawn in the present investigation. A study of the effects of pressure on the structure and properties of molten (equilibrium liquid) $CaAl_2Si_2O_8$ at T = 4000 K (well above the computer glass transition temperature of $T_g \approx 2800$ K) from low pressure to 76 GPa was presented by Nevins and Spera (1998). They found that profound changes in short-range structure and atom mobility occur as pressure increases along the 4000 K isotherm in molten $CaAl_2Si_2O_8$. The abundance of TO_4 and TO_6 (T = Si, Al) polyhedra monotonically decrease and increase, respectively, as pressure increases, whereas the concentration of distorted trigonal bipyramids of pentahedrally coordinated T (TO_5) goes through a maximum at 5 GPa. Interestingly, at ~ 5 GPa, all atoms attain global maxima in tracer diffusivity. This, together with the observation of comparably large (~20 to 30 cm^3/mol) activation volumes for all atoms, suggests cooperative atomic mobility in the equilibrium liquid. They also noted significant changes in the oxygen about oxygen and oxygen about T coordination on increasing pressure along the 4000 K isotherm. The former changes rapidly in the 0- to 10-GPa range, whereas the latter exhibits a broad peak in $^{[3]}O$ (i.e., oxygen with three nearest T neighbors as in the stishovite structure) around 40 GPa that reflects the increasing proportion of TO_6 polyhedra as pressure increases. The formation of significant amounts of TO_n (n = 5, 6) polyhedra drastically alters medium-range (0.5 to 1.5 nm) structure by frustration of corner-sharing TO_4 ring formation. Because simulations preformed by Nevins and Spera (1998) were carried out isothermally, neither the temperature dependence of the short-range structure of equilibrium liquid nor the glass transition could be studied.

In the study of Morgan and Spera (2001), changes in the structure, thermodynamic, and tracer diffusive properties of $CaAl_2Si_2O_8$ at temperatures corresponding to the equilibrium liquid through the metastable supercooled liquid state, and finally to the nonequilibrium glass were explored along the ~ 1-GPa isobar. The computer glass transition was detected as a break in slope of molar enthalpy (H) vs. temperature at $T = T_g \approx 2800$ K. The difference in isobaric heat capacity between supercooled melt and glass at T_g was found to be 53.3 J/K mol, in fair agreement with the calorimetric value when adjusted for the lower temperature of the laboratory glass transition at T = 1160 K. The computer isobaric heat capacity for equilibrium liquid at 3000 K of 457 ± 35 J/K mol is identical, within error, to the calorimetric value of 461 J/K mol. They also showed that speciation in the equilibrium liquid (i.e., for T > 2800 K) defined by reactions $^{[1]}O + {}^{[3]}O = 2\ {}^{[2]}O$ and $TO_4 + TO_6 = 2\ TO_5$ were characterized by the thermodynamic parameters ΔH and ΔS approximately equal to −39 kJ/mol and 19 J/mol K and −10 kJ/mol and 12 J/mol K, respectively, in good agreement with the laboratory value of −35 kJ/mol for the enthalpy of the oxygen speciation reaction. They noted that for T < 2800 K, all speciation equilibria become "frozen." Finally, Morgan and Spera (2001) computed the tracer diffusivity for all atoms in the temperature range of the MD simulations. At fixed temperature, the magnitude of self-diffusivities ordered according to $D_{Ca} > D_O > D_{Al} > D_{Si}$, with D_{Ca} ~ 20% larger than D_O and $D_O \approx 2\ D_{Si}$. Activation energies for diffusion for all atoms were found to lie in the rather restricted range 170 to 190 kJ/mol. The small range in tracer diffusivity, activation energy (E_a) and activation volume (V_a) for all atoms at a given temperature suggests cooperative motion is important in their collective mobility (see also Lesher et al., 1996; Pakula and Teichmann, 1997; Bryce et al., 1999).

Table 1. Potential parameters.

Species *i*	Species *j*	A_{ij} (× 10^{-9} erg)	B_{ij} (× 10^8 cm^{-1})
Ca	Ca	15.387	3.4483
Al	Ca	7.7528	3.4483
Al	Al	3.8831	3.4483
Si	Al	3.7906	3.4483
Si	Ca	7.6069	3.4483
Si	O	3.1295	3.4483
Si	Si	3.6839	3.4483
O	Ca	5.9082	3.4483
O	Al	3.0913	3.4483
O	O	1.7014	3.4483

2. MATERIALS AND METHODS

The MD simulations were performed on IBM RS 6000-43P and RS 6000-350 workstations by use of FORTRAN algorithms developed from Allen and Tildesley (1987) by Rustad et al. (1990) and modified by Stein and Spera (1995, 1996). Further details may be found in Stein and Spera (1995), Nevins and Spera (1998), Bryce et al. (1999), and Morgan and Spera (2001). A simple pairwise additive intermolecular potential containing Coulomb interactions and exponential Born-Mayer-Huggins repulsion was used: $U_{ij} = q_i q_j / r_{ij} + A_{ij} \exp(-B_{ij} r_{ij})$. The size and softness parameters found in Scamehorn and Angell (1991) have been mapped into the form of A_{ij} and B_{ij} (see Table 1), where the full ionic charge between particle i, q_i and particle j, q_j is separated by the interparticle distance r_{ij}. The Ewald method was used to compute the Coulomb interaction for each ion, and a cutoff of 8 Å was used in evaluation of repulsive forces. The gaussian distribution canceling parameter, κ, was set to 5/L, where L is the length of the primary MD cubic box edge. The sum over the reciprocal lattice vectors $\mathbf{k} = 2\pi\mathbf{n}/L$ were determined for all $|\mathbf{n}|^2 \leq 81$. Most simulations were performed with 1300 particles for 50 ps at 1-fs time steps. Two simulations (T = 2670 and 3475 K) were carried out to 150 ps with N = 1300 particles to study relaxation at longer times. All production run simulations were performed in the fixed number, volume, and energy microcanonical ensemble and momentum and energy were conserved to greater than one part in 10^5. The temperature, pressure, density, energy (total and potential), and simulation durations are listed in Table 2. Typical temperature fluctuations are ~50 K; the pressure fluctuations are ~0.7 GPa. The average pressure of 17 simulations is

Table 2. Molecular dynamics simulation physical data summary: $CaAl_2Si_2O_8$.

T (K)	P (GPa)	ρ (kg/m^3)	Total Energy (kJ/mol)	Potential Energy (kJ/mol)	Duration (ps)
1707 ± 29	1.32 ± 0.45	2605	-4.246×10^4	$-4.274 \times 10^4 \pm 7.210 \times 10^2$	50
1871 ± 33	0.45 ± 0.55	2503	-4.239×10^4	$-4.271 \times 10^4 \pm 7.443 \times 10^2$	50
2013 ± 37	1.20 ± 0.51	2559	-4.235×10^4	$-4.269 \times 10^4 \pm 7.778 \times 10^2$	50
2239 ± 40	0.88 ± 0.57	2495	-4.227×10^4	$-4.265 \times 10^4 \pm 7.555 \times 10^2$	50
2320 ± 41	1.00 ± 0.56	2561	-4.224×10^4	$-4.263 \times 10^4 \pm 7.412 \times 10^2$	50
2542 ± 46	1.18 ± 0.59	2553	-4.215×10^4	$-4.258 \times 10^4 \pm 7.566 \times 10^2$	50
2670 ± 50	1.04 ± 0.60	2504	-4.212×10^4	$-4.256 \times 10^4 \pm 7.871 \times 10^2$	150
2868 ± 58	1.15 ± 0.66	2502	-4.203×10^4	$-4.251 \times 10^4 \pm 8.478 \times 10^2$	50
2947 ± 51	0.86 ± 0.65	2448	-4.200×10^4	$-4.248 \times 10^4 \pm 7.271 \times 10^2$	50
3086 ± 60	1.03 ± 0.70	2466	-4.194×10^4	$-4.245 \times 10^4 \pm 8.034 \times 10^2$	50
3150 ± 57	1.24 ± 0.71	2465	-4.192×10^4	$-4.244 \times 10^4 \pm 7.539 \times 10^2$	50
3475 ± 62	1.12 ± 0.71	2458	-4.178×10^4	$-4.235 \times 10^4 \pm 7.435 \times 10^2$	150
3481 ± 62	1.17 ± 0.73	2465	-4.177×10^4	$-4.234 \times 10^4 \pm 7.431 \times 10^2$	50
3983 ± 72	1.33 ± 0.75	2434	-4.156×10^4	$-4.223 \times 10^4 \pm 7.469 \times 10^2$	50
4151 ± 72	0.17 ± 0.78	2465	-4.150×10^4	$-4.218 \times 10^4 \pm 7.239 \times 10^2$	50
4500 ± 41	1.88 ± 0.81	2465	-4.135×10^4	$-4.208 \times 10^4 \pm 3.743 \times 10^2$	50
4976 ± 87	0.85 ± 0.81	2466	-4.115×10^4	$-4.196 \times 10^4 \pm 7.324 \times 10^2$	50

1.05 GPa with a standard deviation (1σ) of 0.37 GPa, smaller than typical pressure fluctuations during a single run.

The cooling schedule involved an initial system of 100 Ca, 800 O, and 200 Al and 200 Si ions randomly configured at T ~ 100,000 K. Large intermolecular potential forces were allowed to relax for a period of 10 ps before the system was quenched to 10,000 K at rate γ = dT/dt = 10,000 K/ps by velocity scaling. Excess momentum in the system was then removed and the system equilibrated for 10 ps. From 10,000 K, a configuration at 3000 K and 1.35 GPa was obtained with a temperature quench rate of 700 K/ps and a pressure quench rate (dP/dt) of 1 GPa/ps. This configuration at 3000 K was the initial configuration for all production runs. To remain along the isobar, the system was either cooled or heated at a quench rate γ = 70 K/ps isobarically. Once the desired temperature was achieved and velocity scaling turned off, a 50- or 150-ps number, volume, and energy production simulation was performed. These production trajectories represent the data analyzed in the sections below.

3. RESULTS

3.1. Tracer Diffusivity: Three Regimes

The tracer or self-diffusivity of a particular atom type (e.g., oxygen or silicon) is a collective property representing a coarse-grained or statistical measure of an underlying microscopic process—the "simple" motion of an individual atom. Circumstantial evidence summarized above suggests atomic diffusion is cooperative in $CaAl_2Si_2O_8$ on the basis of the similarity of the magnitude of self-diffusion coefficients, activation energies, and activation volumes for O, Ca, Si, and Al. In what follows, we look more deeply into this issue to better understand the mechanism of diffusion and to investigate behavior as a function of temperature near the glass transition. This is the essence of the glass transition problem because viscous flow implies some sort of material transport.

Tracer diffusivity (D_i) for each atom is computed from the mean square displacement (MSD) of a tagged particle averaged over all atoms of the same type over the duration of the simulation. By use of the Einstein relation (random walk), the tracer or self-diffusivity for the *i*th ion is

$$D_i = \lim_{t\to\infty} \frac{\langle |\mathbf{r}_i(t) - \mathbf{r}_i(0)|^2 \rangle}{6t} \quad (1)$$

where the numerator is the MSD of the *i*th ion and the brackets imply an average over an equilibrium ensemble or, equivalently by invoking ergodicity, over a set of initial times sampled from the run after it has reached equilibrium. In this study, 100 time origins were used in Eqn. 1. Tracer diffusivities for Ca, Al, Si, and O at representative temperatures spanning the glass transition are plotted in Figure 1, which shows the variation of the MSD of a particle vs. time. Note this is a logarithmic plot with timescale varying from the femtosecond, corresponding to quasilattice vibration, to ~100 ps; MSDs exceed 100 Å^2 for calcium and oxygen atoms at high temperature.

Three distinct transport regimes are identified for each atom on Figure 1. At very short times, atoms move along ballistic paths and the square of the mean particle displacement scales as MSD ~ t^2. This behavior is noted in Figure 1 at all temperatures and all atoms to ~5 fs and shows the dominating effects of inertia at small time as atoms fly on ballistic trajectories. In contrast, at longer times, atomic mobility depends markedly on temperature. At high temperatures, in the normal liquid range ($T \gg T_g$) Einstein random walk governs atomic motion. For times greater than ~10 ps, MSD ~ t. This is observed on Figure 1 at high temperature for all atoms, even the least mobile ones, silicon and aluminum (Figs. 1b,c). As T decreases toward T_g, a dramatic change occurs. A "plateau" region of subdiffusion occurs, and the duration of the plateau interval increases as temperature is lowered. At $T \approx T_g$, for example, a well-developed plateau is apparent for all atoms in the approximate time window 0.1 to 10 ps. At $T < T_g$, the plateau extends out to 20 to 30 ps for calcium and ~50 ps for slow-moving silicon. The correlation MSD ~ t^β, where β is an increasing function of temperature, holds very roughly for $t > \sim 0.1$ ps. The power-law exponent β goes to unity in the limit $t \to \infty$ 3 for $T > T_g$. In detail, a more complex variation of MSD with time is noted from Figure 1. At ~5000 K, the result expected for hydrodynamic diffusion (uncorrelated random walk), MSD ~ t is attained at t > 10 ps. In contrast, at low temperature (1700 K), the subdiffusive regime dominates

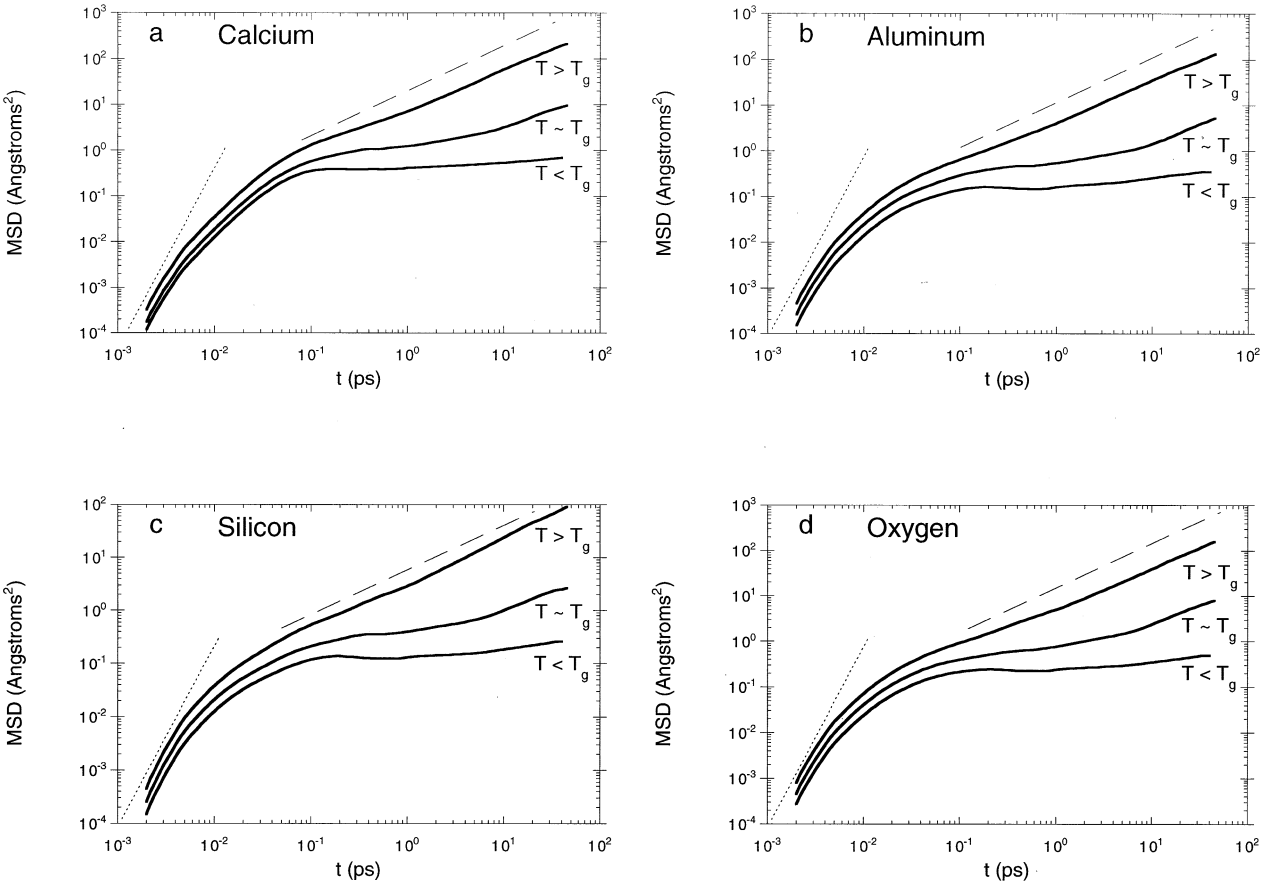

Fig. 1. Logarithmic plot of the MSD vs. time illustrating the ballistic, subdiffusive and diffusive regime (see text). The dotted line (slope of two) and the dashed line (slope of one) are included to differentiate the regimes. The average temperatures of the simulations are 1713, 2884, and 4956 K, bottom to top, spanning the (computer) T_g.

and extends out beyond 50 ps, the time limit of Figure 1. Accurate assessment of the relationship between the MSD and time awaits further study especially at long times and low temperature. Horbach et al. (1998) found similar results for amorphous silica studied by MD simulation.

A qualitative microscopic interpretation of atomic diffusion in $CaAl_2Si_2O_8$ focusing on oxygen may be offered. Oxygen becomes temporarily trapped in cages defined by the oxygen, T, and Ca sublattices for increasing periods as temperature drops. The short-range structure defining these coordination cages was characterized in detail in the study of Morgan and Spera (2001). The vibration of oxygen in this trapped mode contributes little to its MSD (see Fig. 1d). As temperature increases, distinguishing the motion of oxygen within a cage from the jump motion becomes difficult. The primary qualitative feature is that a given particle, and its neighbors remain trapped for a finite period before undergoing a thermally activated hop. Furthermore, the jump motion entails a cooperative rearrangement among at least several atoms because the atoms defining a coordination cage are themselves caged. The distribution of "waiting times" is strongly temperature dependent and related to the dramatic increase in structural relaxation time as temperature approaches T_g.

3.2. van Hove Self-Correlation Function

Further insight into the microscopic dynamics of diffusion is garnered by study of the self part of the van Hove correlation function, defined as

$$G_s(r,t) = \frac{1}{N}\left\langle \sum_{i=1}^{N} \delta[r - |\mathbf{r}_i(0) - \mathbf{r}_i(t)|] \right\rangle. \quad (2)$$

The function $P(r,t) = 4\pi r^2 G_s(r,t)$ gives the likelihood that a particle at $r = 0$ at $t = 0$ has moved a distance r in time t. For Fickian diffusion in an equilibrium liquid, $G_s(r,t)$ decays to zero as $t \rightarrow \infty$ and large distances according to the classical gaussian hydrodynamic relation:

$$G_s(r,t) = \frac{1}{(4\pi D_i t)^{2/3}} \exp\left(-\frac{r^2}{4D_i t} \right), \quad (3)$$

where D_i is the tracer diffusivity of the *i*th ion. When diffusion occurs by jumps or hops to nearest neighbor sites, P(r,t) exhibits a multipeaked structure. Such structure is expected as T_g is approached because the waiting time between successive hops of a particle becomes comparable (although still shorter than) the duration of the simulation.

In Figures 2 to 5, P(r,t) is plotted for calcium, oxygen,

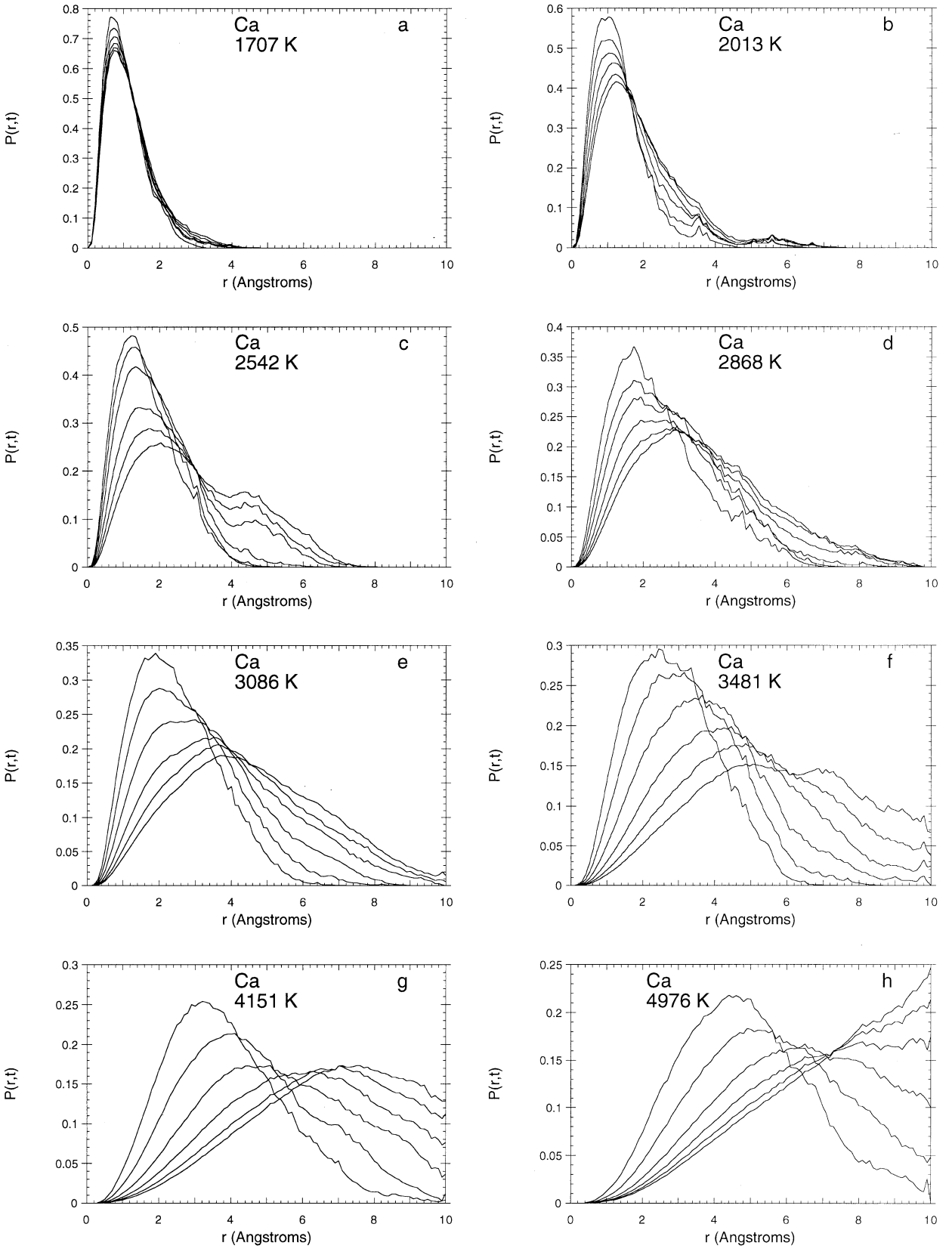

Fig. 2. van Hove correlation function for calcium, $4\pi r^2 G_s(r,t)$. P(r,t) vs. radial distance, r for times, t = 2.5, 5, 10, 20, 30, and 40 ps. P(r,t = 2.5 ps) has the largest amplitude on all plots. (a) T = 1707 K. (b) T = 2013 K. (c) T = 2542 K. (d) T = 2868 K. (e) T = 3086 K. (f) T = 3481 K. (g) T = 4151 K. (h) T = 4976 K.

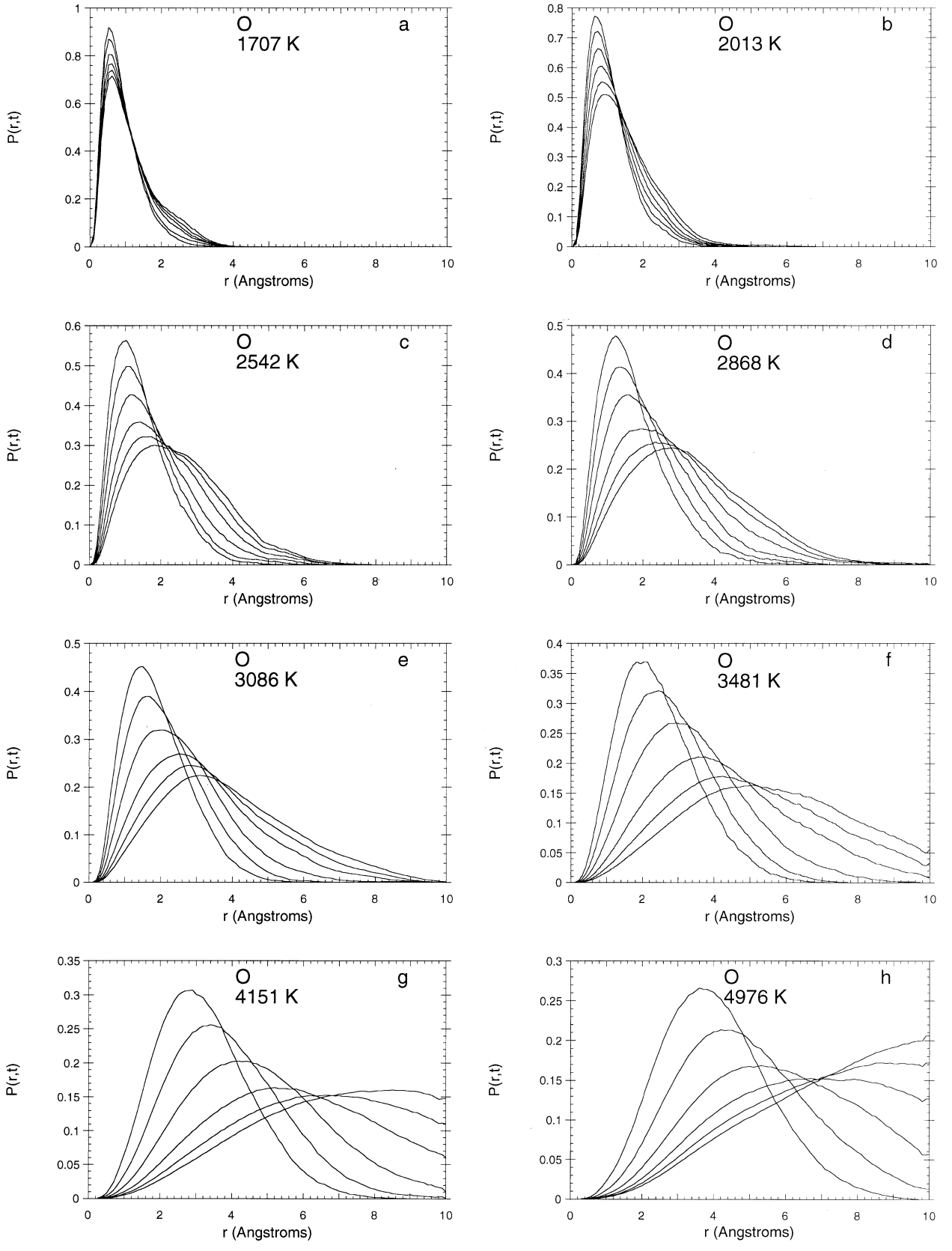

Fig. 3. van Hove correlation function for oxygen, $4\pi r^2 G_s(r,t)$. See Figure 2 legend for details.

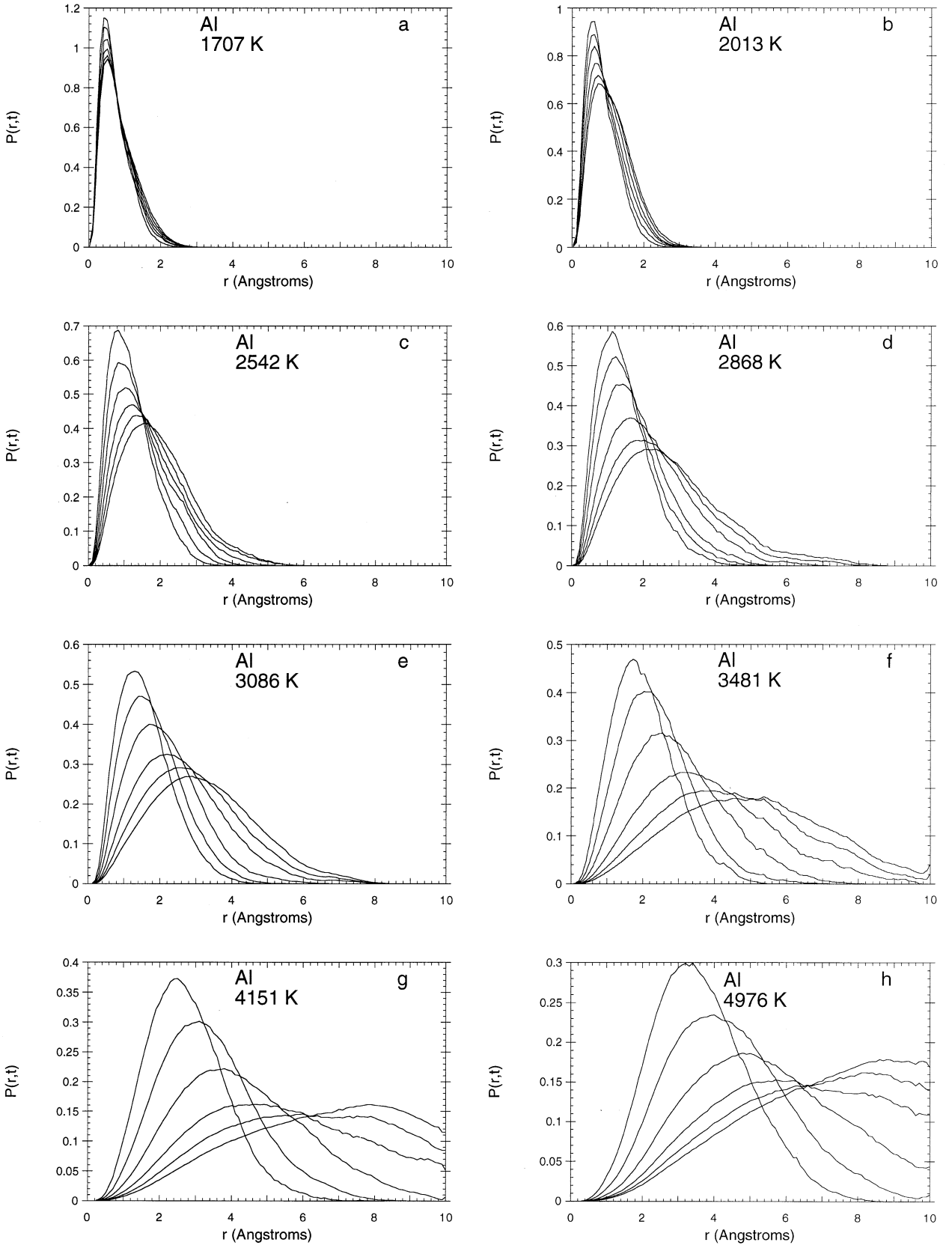

Fig. 4. van Hove correlation function for aluminum, $4\pi r^2 G_s(r,t)$. See Figure 2 legend for details.

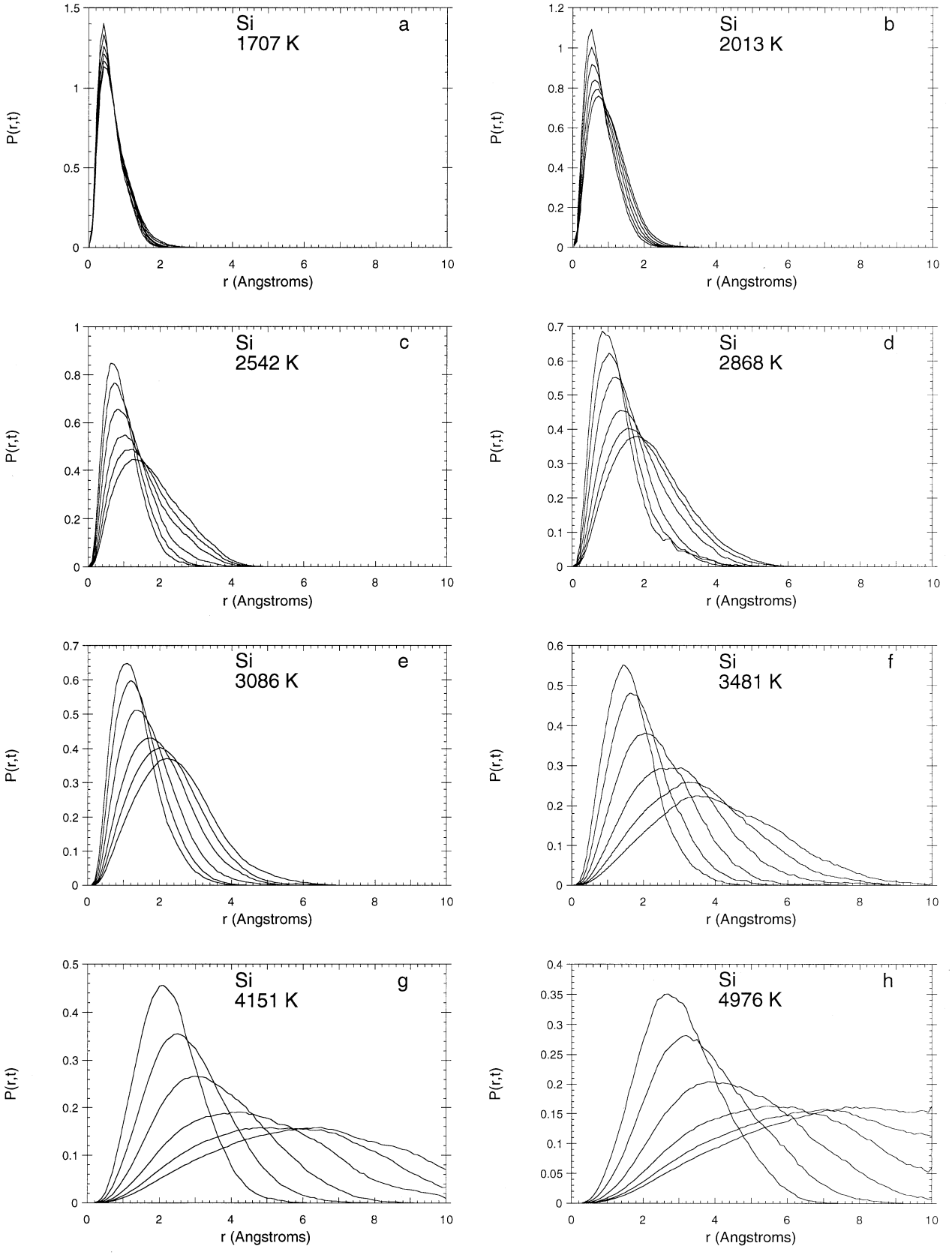

Fig. 5. van Hove correlation function for silicon, $4\pi r^2 G_s(r,t)$. See Figure 2 legend for details.

aluminum, and silicon against r at various times for temperatures spanning the glass transition. Inspection of these plots reveals important features of the dynamics of atomic-scale diffusion in $CaAl_2Si_2O_8$. The discussion below is based on examination of van Hove correlation plots for all temperatures listed in Table 2. For brevity, only a representative sampling of these temperatures is included in Figures 2 to 5.

In Figure 2, the self part of the van Hove correlation function for calcium is shown for temperatures between 1707 and 4976 K. At 1707 K, there is little change in the r value of the first peak, although the amplitude of the maximum decays as time progresses. At T = 2320 K (data not shown), a broad shoulder develops at $t \sim 30$ ps at $r \approx 4.5$ Å, corresponding roughly to the distance between second-nearest neighbor calcium atoms. At T = 2542 K, the shoulder develops into a second peak by t = 20 ps. This is evidence for calcium hopping (jump motion) between oxygen-defined caged sites (see fig. 4a in Morgan and Spera, 2001). At $T > 2500$ K, the first peak of the van Hove correlation function begins to show significant migration as time increases. Around T_g (2600 to 3000 K), the distinctness of the second peak is muted by the migration of the first peak for $t > 30$ ps. Finally, at $T \gg T_g$, P(r,t) takes on the form expected for equilibrium liquids: a single peak that rapidly decays shifting to increasing r as $t \rightarrow \infty$.

The evolution of the oxygen P(r,t) is traced from 1707 to 4976 K in Figure 3. The overall progression is similar to that for calcium, although the development of the second "hopping" peak is somewhat muted. At 1707 to 2013 K, there is little peak migration at least until 40 ps, and a small shoulder around $r \approx 2.7$ Å (close to the average first neighbor O-O separation) develops on the tail of P(r,t). At higher temperatures (2320 to 2670 K), the amplitude of the shoulder first grows and then amalgamates with the primary peak that migrates to larger distances. Figure 3d (T = 2868 K) exhibits the characteristics of an equilibrium liquid with a typical gaussian van Hove probability distribution. T_g is located roughly around 2800 K on the basis of van Hove analysis of oxygen mobility. The conspicuous shoulder apparent in Figures 3a–c indicates that jump motion contributes substantially to oxygen mobility.

The van Hove correlation functions for aluminum (Fig. 4) and silicon (Fig. 5) are similar; discussion here is limited to silicon. For $T < 2500$ K, there is little migration of the P(r,t) peak position, consistent with the frozen structure at $T < T_g$. A key difference between both Al and Si compared with Ca and oxygen is the lack of a shoulder or second peak in the P(r,t) at $T < T_g$. This indicates that hopping is less frequent for Al and Si compared with oxygen and calcium. In terms of the MSD vs. t relationship in Figure 1, the duration of the subdiffusive regime is longer for Si and Al compared with the more mobile Ca and O.

In summary, analysis of the van Hove correlation function, specifically its dependence on temperature, enables one to differentiate the frozen from unfrozen (ergodic) state. At low temperature ($T < T_g$), the bimodal form of P(r,t) indicates an important role for jumps in explaining atomic mobility. Jumps probably remain important for $T > T_g$, but jump motion becomes difficult to separate from cage drift when the displacement of an atom as a result of cage drift becomes comparable to the MSD associated with "out-of-cage" cooperative hopping.

3.3. Self-Intermediate Scattering Functions

Scattering functions were computed from MD data that used particle locations as a function of time. The time evolution of this density–density correlation function provides information regarding the spatial and temporal decay of density fluctuations expressed in terms of Fourier components, ρ_k, of the instantaneous number density of the different atoms making up the material. The number density (collective) autocorrelation function is defined as:

$$F_{NN}(k,t) = \frac{1}{N}\langle \rho_k(t)\rho_{-k}(t)\rangle \tag{4}$$

where $\mathbf{k}$ is the wave vector, $k = \mathbf{k}$, and $\rho_k(t)$ is a Fourier component of the instantaneous microscopic density defined as

$$\rho_k(t) = \sum_{j=1}^{N} \exp\left[ik\cdot r_j(t) \right] \tag{5}$$

(Hansen and McDonald, 1986). The brackets in Eqn. 4 imply an ensemble average has been taken. The "self" part of the scattering function, where only one type of atom is considered, is more accurately computed than the nonself part because of better sampling statistics. Here we focus wholly on the self-intermediate scattering function defined:

$$F_s^{(\alpha)}(k,t) = \frac{1}{N_{(\alpha)}}\sum_{j=1}^{N_{(\alpha)}}\langle \exp\{i\mathbf{k}\cdot[\mathbf{r}_j(t) - \mathbf{r}_j(0)]\}\rangle, \tag{6}$$

with $\alpha \in$ {Ca, Al, Si, O}. In general, the decay rate of the scattering function increases with k because short wavelength fluctuations in microscopic density die out more rapidly than longer ones. $F_s(k,t)$ provides information regarding the temporal decay of microscopic "same-atom" density fluctuations as a function of spatial scale (monitored by k, the wave vector) and temperature.

It is helpful to study the time dependence of the scattering function at a fixed k. Typically one chooses the value of k at which the partial static structure factor, $S_\alpha\alpha(r)$, defined

$$S_{\alpha\alpha}(k) = 1 + 4\pi\frac{N_\alpha}{V}\int_0^\infty (g_{\alpha\alpha}(r) - 1)\frac{\sin(kr)}{kr} r^2 dr \tag{7}$$

attains a maximum (k_{max}). The static structure factor S(k) is closely related to the intermediate scattering function in that the later is just a time-dependent generalization of the former, e.g., $S(k) = F_s(k,0)$. In Eqn. 7, $g_\alpha\alpha(r)$ is the self-atom pair correlation function and N_α is the number of atoms of type α. For example, the value is $k_{max} = 2.64$ Å^{-1} for oxygen (Fig. 6d). Physically, this corresponds to a distance $r \sim 2\pi/k_{max} \sim 2.4$ Å, roughly the distance of the first peak in the oxygen–oxygen pair correlation function, $g_{OO}(r)$ (Morgan and Spera, 2001). The static partial structure factor is plotted for all atoms and representative temperatures in Figure 6.

The self part of the intermediate scattering function for all atoms computed from Eqn. 6 at appropriate k_{max} (from Fig. 6) is plotted against the logarithm of time for all simulations (Table 2) in Figure 7. As T_g is approached, the scattering function decays qualitatively differently compared with equilibrium liquid. In all cases, at very short times (<0.2 fs), F_s approaches unity because every atom is localized at its origin at

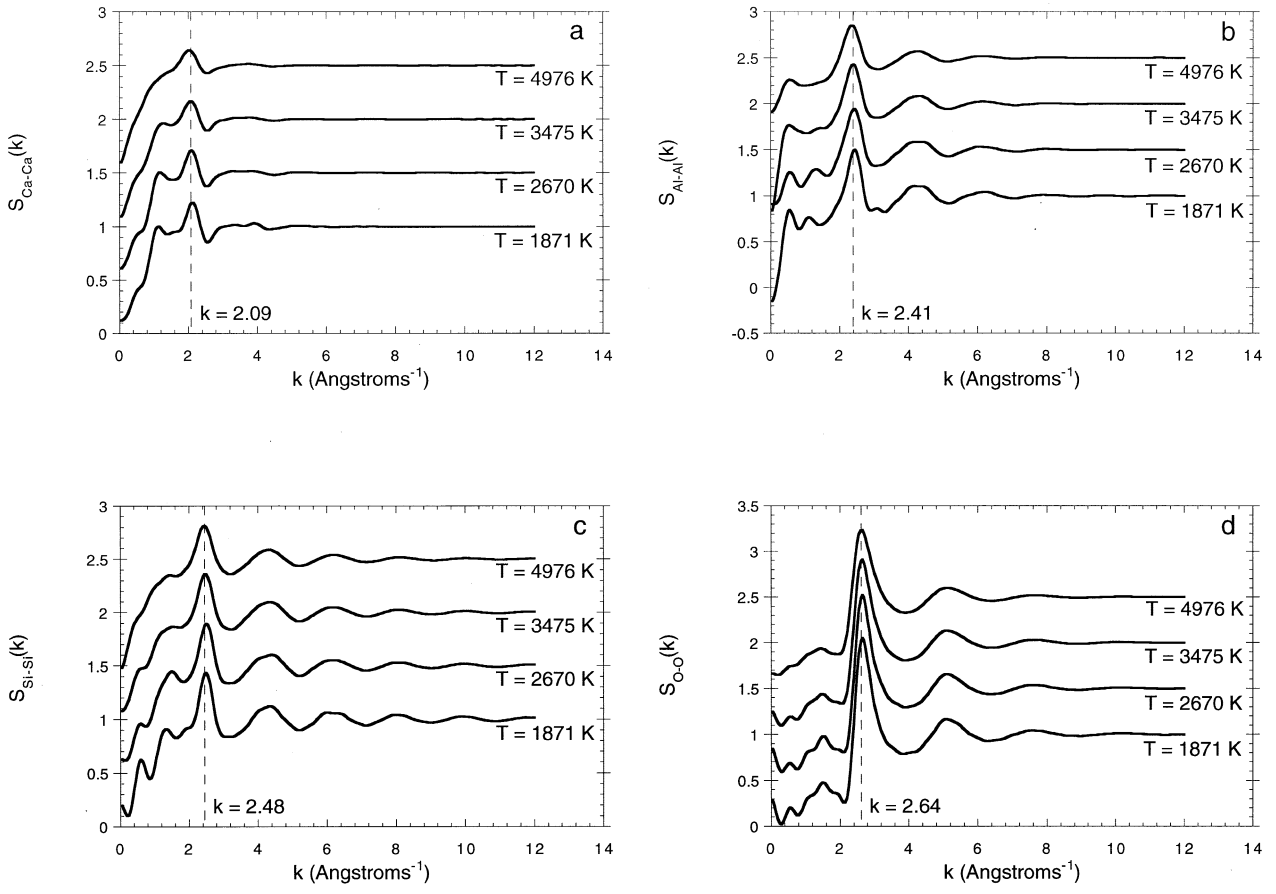

Fig. 6. Partial static structure factor $S_{\alpha\alpha}(k)$ vs. wave vector at temperatures spanning the range of the MD simulations (1871, 2670, 3475, and 4976 K). Curves are offset vertically for clarity and the vertical lines indicate k_{max}. (a) $S_{CaCa}(k)$. (b) $S_{AlAl}(k)$. (c) $S_{SiSi}(k)$. (d) $S_{OO}(k)$. The large amplitude peak at 2.64 $Å^{-1}$ corresponds to the first peak in the oxygen–oxygen pair correlation maximum at approximately 2.7 Å.

$t = 0$. As time evolves and the atom begins to move away from its initial location, $F_s(k,t)$ decreases monotonically.

At high temperatures, the decay is describable by a single relaxation time characteristic of Debye exponential relaxation in an equilibrium liquid (Fig. 7). The time at which the scattering function decays to its asymptotic limit of zero is ~2 ps for all species found from computing Eqn. 6 at the peak in the static partial structure factor for each atom. Otherwise, if $F_s(k,t)$ was computed for the same k_{max} for all the species, such as 2.64 $Å^{-1}$, the fast-moving oxygen and calcium would decay to zero a factor of three or so faster than slower-moving aluminum and silicon. The slow relaxation at temperatures near and below the glass transition temperature of 2800 K is of a stretched exponential form. The behavior of $F_s(k,t)$ at long times is critical to theories of structural relaxation and is discussed below. First, it is useful to introduce a statistical parameter that serves as a measure of the importance of the subdiffusive regime prominently displayed in Figure 1.

3.4. Cumulant Expansion and the First Nongaussian Parameter

A truncated cumulant expansion for the scattering function in powers of k^2 can be written (Rahman et al., 1962)

$$F_s^{(\alpha)}(k,t) = \exp\left\{ -\frac{1}{6}k^2 R_{(\alpha)}(t) + \frac{1}{72}k^4 [R_{(\alpha)}(t)]^2 A_{(\alpha)}(t) + O(k^6) \right\} \tag{8}$$

with

$$A_{(\alpha)}(t) = \frac{3}{5}\frac{\langle |\mathbf{r}_{i\alpha}(t) - \mathbf{r}_{i\alpha}(0)|^4 \rangle}{[R_\alpha(t)]^2} - 1. \tag{9}$$

$A_\alpha(t)$ is the first nongaussian parameter of the cumulant expansion, $R_{(\alpha)}(t)$ is the mean-square displacement (MSD) of species α ($\alpha\varepsilon$\{Ca, Al, Si, O\}), and the numerator of Eqn. 9 is the fourth moment of the displacement (mean quartic displacement). The point of performing the cumulant expansion is that the scattering function is naturally broken up into its gaussian and nongaussian parts. The gaussian part is associated with Debye exponential relaxation and is consistent with "normal" diffusion determined from classical hydrodynamics, giving the well-known relation MSD ~6 Dt. For an equilibrium liquid, the first nongaussian term in the cumulant expansion decays to zero after passing through a maximum at a time that increases as temperature decreases. For example, at 4976 K, $A_O(t)$ maximizes at $t \sim 0.5$ ps, whereas $A_O(t)$ attains a maximum at ~3 ps at 3086 K (Fig. 9). In equilibrium liquids, atoms explore all

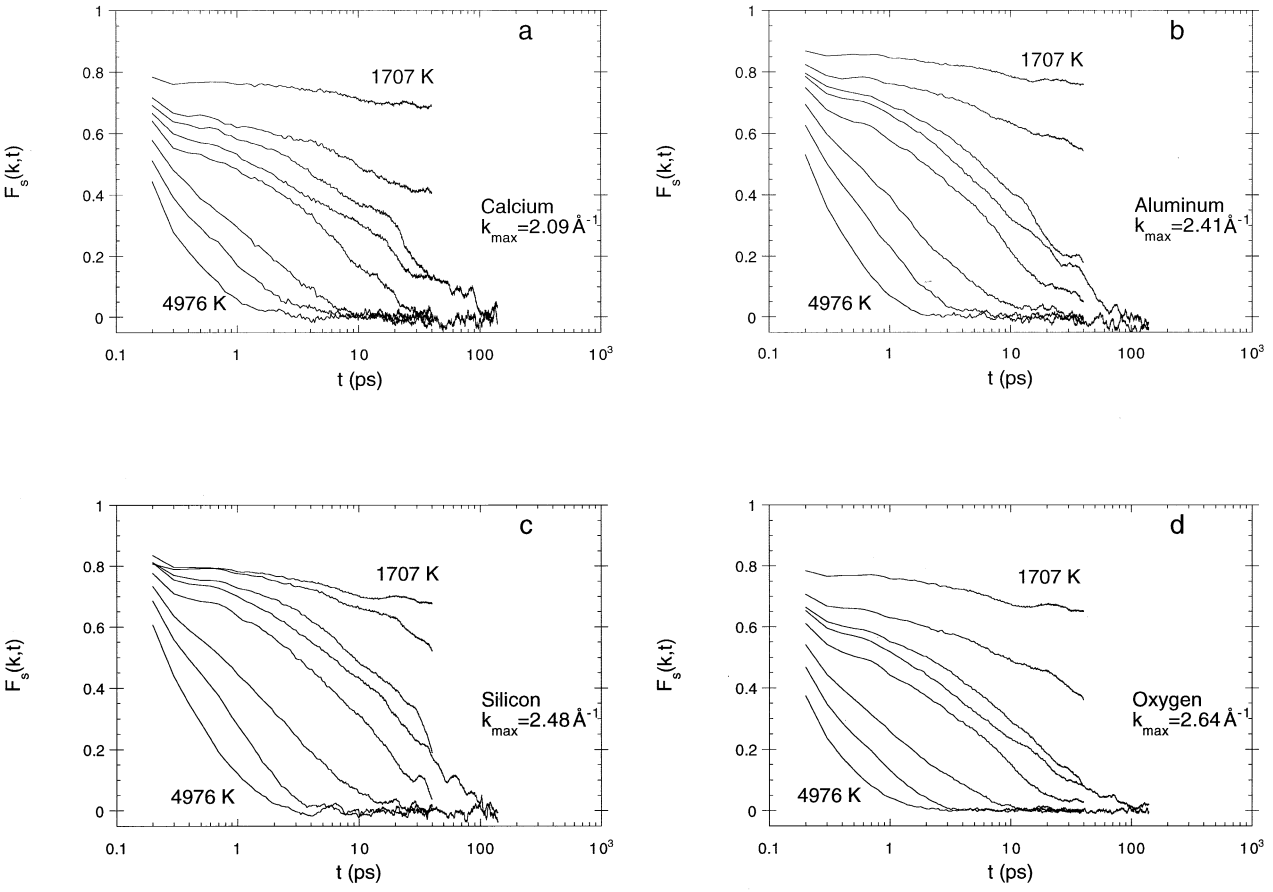

Fig. 7. Intermediate scattering function for (a) calcium, (b) aluminum, (c) silicon, and (d) oxygen vs. time computed at k_{max} found from the maxima of $S_{\alpha\alpha}(k)$ for temperatures: 1707, 2239, 2542, 2670, 2947, 3475, 4151, and 4976 K. At high temperatures, the decay of $F_s(k,t)$ is characterized by exponential relaxation with a single time constant. As temperature is lowered, a single relaxation time no longer captures the decay of the scattering function. The appearance of temporal heterogeneity in the relaxation of microscopic density fluctuations is a defining characteristic of the glass transition.

parts of the phase space on experimental timescales and ergodicity is obeyed. In contrast, in structurally arrested $CaAl_2Si_2O_8$, there is a significant component of nongaussian behavior to the decay of the scattering function. This is noted in Figure 7 at temperatures $T < T_g$ (e.g., at T = 1707 K). Hiwatari et al. (1991) (see also Odagaki et al., 1997) proposed that the asymptotic ($t \rightarrow \infty$) behavior of $A_\alpha(t)$ could be used as an order parameter for the glass transition viewed as a second-order thermodynamic transition (see discussion below).

In Figures 8 to 11, $A_\alpha(t)$ is plotted vs. the logarithm of time for all atoms at temperatures spanning the glass transition. Collectively, Figures 8 to 11 demonstrate some important features of relaxation dynamics reflected by the nongaussian parameter $A_\alpha(t)$. For brevity, discussion is focused on the nongaussian parameter for oxygen (Fig. 9); Ca, Al, and Si show similar behavior and are discussed later.

The behavior of $A_O(t)$ strongly depends on temperature. At all temperatures, $A_O(t)$ initially increases at short times ($t < 1$ ps), reflecting vibration of oxygen around local positions. This motion corresponds to the steep slope of ~2 on the MSD curves in Figure 1. At temperature well above T_g (e.g., 4976 K), the maximum value of $A_O(t)$ occurs, at times on the order of 1 ps or less. The time at which maximum in $A_O(t)$ takes place increases as temperature decreases. For example, at T = 3086 K, $A_O(t)$ attains its maximum value at ~4 ps. At temperatures near the glass transition, the peak in the nongaussian shifts to later times (t ~ 5 to 10 ps). Finally, for $T < T_g$, $A_O(t)$ exhibits more complex behavior with local extrema and evidently no tendency to decay to zero, at least on a 150-ps timescale (e.g., at T = 2670 K; not shown in Figs. 8–11). The extent of nongaussian behavior gauged by both the large magnitude of $A_O(t)$ and its lack of unimodal behavior correlates with the duration of the subdiffusion regime (the plateau region) noted in Figure 1. Although the discussion here focuses on oxygen, Ca, Al and Si exhibit substantially the same behavior (Figs. 8, 10, and 11).

The value of the nongaussian parameter for oxygen at 40 and 140 ps (two temperatures) is shown in Figure 12. At temperatures greater than 3400 K, $A_O(t) \approx 0$, and one can reasonably extrapolate from comparison of the 40- and 140-ps simulations that $A_O(t) \approx 0$ in the limit $t \rightarrow \infty$ for $T > 2800$ K. Below 2670 K, $A_O(t = 40\text{ ps})$ varies systematically with temperature such that the extent of nongaussian behavior increases as temperature decreases. Note that the more slowly cooled simulation

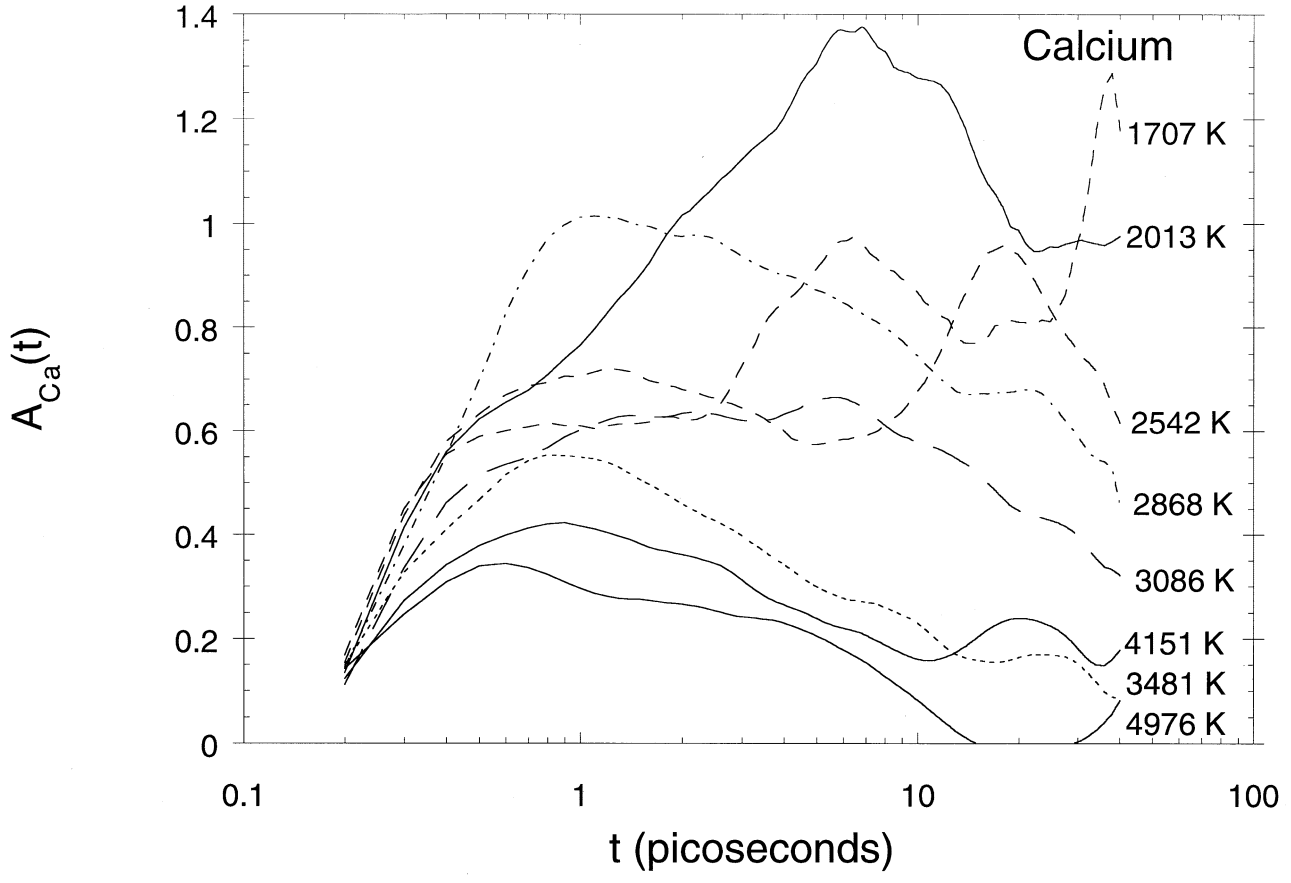

Fig. 8. Nongaussian parameter for calcium, $A_{Ca}(t)$. See text for discussion

(γ = 70 K/ps) at 3086 K is barely distinguishable from the simulation at T = 3150 K, quenched at the higher rate γ = 700 K/ps. The quench rate is not a large factor influencing these results (see Morgan and Spera, 2001, for further discussion of MD quench rate effects). The open squares on the figure at T = 2670 and 3475 K show $A_O(t)$ at = 140 ps; these indicate that 40-ps data are not sufficient to define asymptotic values of $A_O(t \rightarrow \infty)$, although the trend is clearly defined. To verify the asymptotic behavior of $A_O(t)$, longer simulations must be carried out.

Computed values for the oxygen-oxygen scattering function were fit to the Kohlrausch-Williams-Watts (KWW) stretched exponential function:

$$F_s^{(\alpha)}(k,t) = C\, exp\,[-(t/t_o)^{\beta}], \tag{10}$$

where C, t_o, and β are fit parameters. In the hydrodynamic limit (small k), the relaxation time $t_o = t_H = [D_O\, k^2]^{-1}$, where D_O is the temperature-dependent diffusion constant and β = C = 1. The wave vector length used to compute t_H is the smallest one consistent with the length (L) of the simulation box, $k_{min} = 2\pi/L$. Single exponential behavior (β = 1) with a hydrodynamic timescale (t_H) is expected for the equilibrium liquid for which $A_\alpha(t)$ vanishes in the limit $t \rightarrow \infty$. Table 3 collects the best-fit KWW values for oxygen on the basis of the MD simulations, the hydrodynamic approximation to the relaxation time, t_H, and the ratio t_o/t_H. Although somewhat noisy, the high temperature results conform to the hydrodynamic expectation for a liquid (i.e., $t_o/t_H \approx 1$ and $\beta \approx 1$). For T < 2800 K, t_o increasingly deviates from t_H and β values deviate from unity, indicating non-Debye stretched exponential relaxation. In Figure 13, β's determined by the KWW fit (β_{KWW}) and from the MSD analysis of simulations in Table 2 (β_D) are plotted vs. reciprocal temperature normalized by T_g. Because the KWW fit involves retrieval of three parameters simultaneously, it is expected that the MSD-derived values are more accurate.

4. DISCUSSION

4.1. Theories of Viscosity: General Attributes

Many theories have been proposed to account for the dramatic increase in relaxation time and accompanying strong variation in transport properties (e.g., shear viscosity and tracer diffusivity) at the glass transition. Useful reviews of the theory of viscosity and the glass transition include those by Fredrickson (1988), Angell (1988, 1991), Bottinga (1994), Bottinga et al. (1995), Ediger (1996), Debenedetti (1996), and Kob (1999). Here, discussion is restricted to three models of the glass transition, with particular reference to the MD simulations described above.

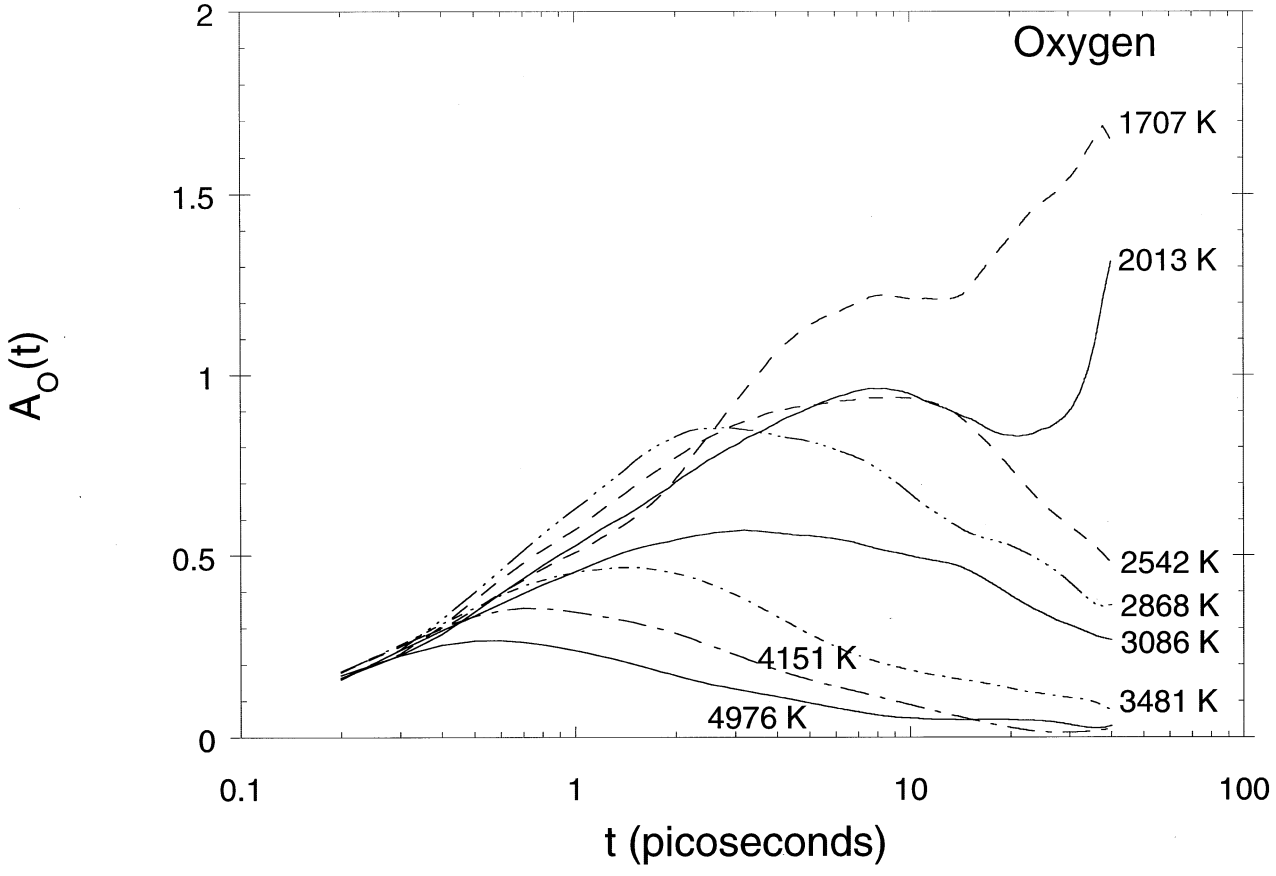

Fig. 9. Nongaussian parameter for oxygen, $A_O(t)$. See text for discussion

Changes in the structure of amorphous $CaAl_2Si_2O_8$ with temperature in the deeply supercooled region appear insignificant around T_g. (Fig. 6; see also Morgan and Spera, 2001). The static structure factors for many other supercooled liquids likewise provide no evidence for a growing static length scale near T_g. The glass transition is therefore a dynamic rather than static structural transition. Indeed, the large increase in structural relaxation time, reflected by large changes in shear viscosity around T_g, is a universal feature of the glass transition common to many different kinds of materials. The search for a growing dynamic-length scale ties together many theories of the glass transition and associated theories of viscosity. Before discussing the various theories in more detail, we present a general picture. In a qualitative sense, all viscosity theories discussed in detail below share (more or less) these features.

Supercooled liquids, by virtue of their high densities, place strong frustration constraints on the dynamics of individual atoms. As temperature decreases toward T_g, a tagged atom is more likely to be trapped by neighbors (i.e., caged) because the amplitude of thermodynamic fluctuations (e.g., internal energy and kinetic energy) decrease as temperature decreases. Near T_g, a caged particle may remain trapped for relatively long times. Liberation of the imprisoned particle requires cooperative rearrangement of a number of atoms surrounding the tagged particle because neighboring atoms making up the cage are themselves caged and must move as well. In a multicomponent network material such as $CaAl_2Si_2O_8$, topological frustration is enhanced by the presence of particles of different effective size and charge. The volume over which cooperative motions must occur to relax a cage presumably increases as the temperature decreases. Long times are therefore required for cooperative rearrangements involving large numbers of atoms.

The view of sluggish dynamics in three-dimensional Euclidean space may be augmented by consideration of the dynamics in $6N + 1$ dimensional phase space. The "topographic" viewpoint espoused by Stillinger (1995) is particularly useful. Interaction between particles is described by a potential energy function $\mathbf{\Phi}(\mathbf{r}_1, \mathbf{r}_2, \ldots, \mathbf{r}_N)$, which depends on the location $\mathbf{r}_i$ of each particle in the system. An apt geological analogy is a "topographic" map showing the "elevation" $\mathbf{\Phi}$ at "location" $\mathbf{R} \equiv (\mathbf{r}_1, \mathbf{r}_2, \ldots, \mathbf{r}_N)$ in the 3N-dimensional configuration space of the N particle system. Potential energy basins correspond to mechanically stable arrangements of the N particles, with vanishing force on every particle. Small displacements from this arrangement give rise to restoring forces that return the system to its equilibrium state. It is conjectured that basin minima have a substantial variation in depth and may be arranged in a geometrically complex pattern throughout configuration space. The transition from Debye exponential to stretched exponential relaxation, which from the MD simulations takes place around 2800 K at 1 GPa for $CaAl_2Si_2O_8$, can be interpreted as follows. As temperature declines toward T_g, $\mathbf{R}(t)$ enters an increasingly

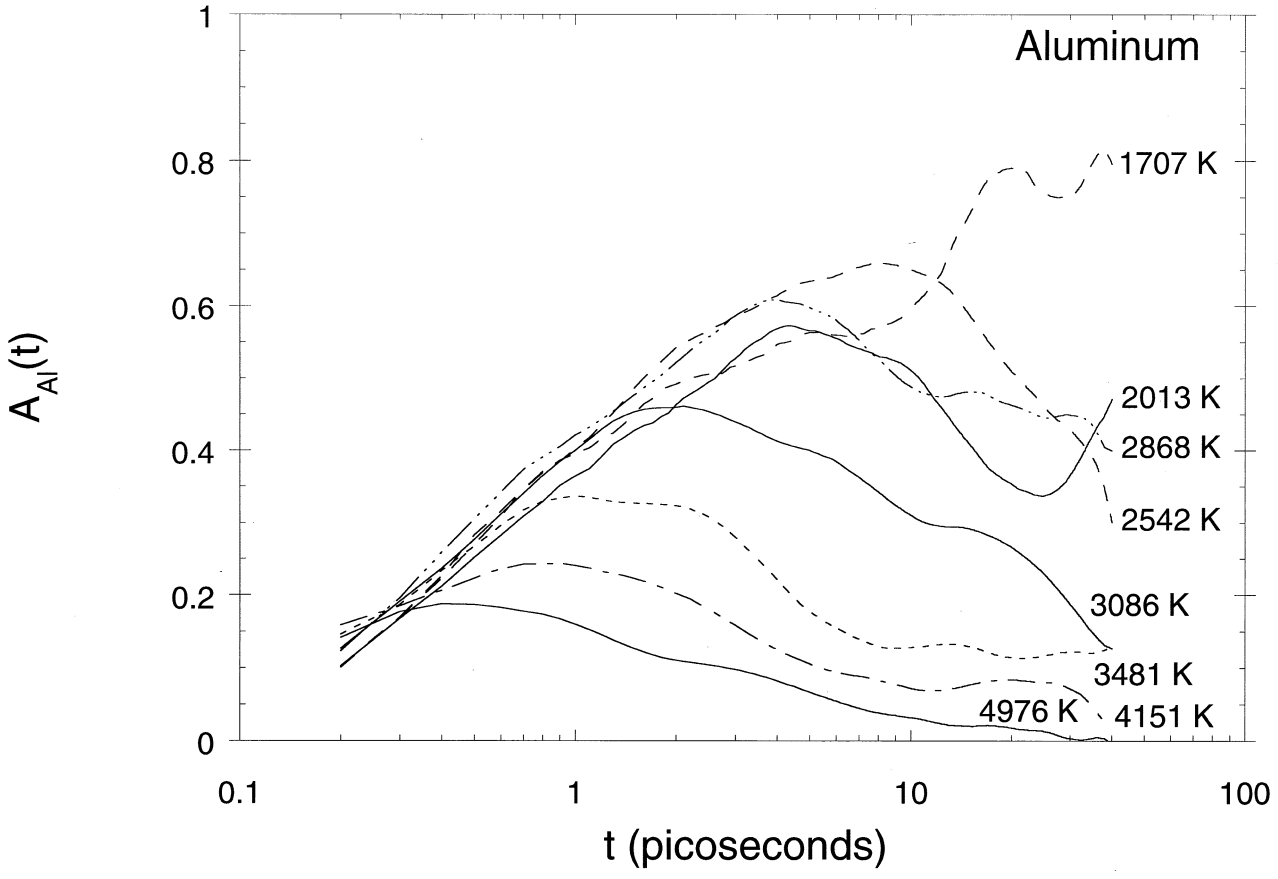

Fig. 10. Nongaussian parameter for aluminum, $A_{Al}(t)$. See text for discussion.

rugged and heterogeneous portion of configuration space as it seeks out ever deepening **Φ**-scape minima. The lower the temperature, the rarer and more widely spaced the megabasins become. Escape from one deep megabasin to another requires many cooperative elementary steps, the integrated sum of which are characterized by large Arrhenian activation energy. However, the elementary transition processes connecting contiguous small basins requires only local rearrangements of small numbers of particles exhibiting Arrhenian-Debye simple relaxation. With this general background in mind, different models of the glass transition are now examined in the context of the MD simulations.

4.2. Configurational Entropy Model

A phenomenological model for the glass transition was proposed over 35 yr ago by Adam and Gibbs (1965). Generally referred to as the AGSC model, critical elements derive from the earlier work of Kauzmann (1948), Gibbs (1956), and Gibbs and DiMarzio (1958) (see also Goldstein, 1969, 1976). In the AGSC theory, the temperature-dependent relaxation time for a viscous material is determined from the probabilities for cooperative rearrangements to take place. Transition probabilities are evaluated by defining a cooperatively rearranging region (CRR) as a sample subsystem that, upon sufficient fluctuation in enthalpy, can rearrange into another configuration independent of the environment. The number of atoms in a CRR is taken as z, and among all subsystems, the fraction of subsystems in a state permitting rearrangements (transitions) is $\Omega = \exp[-z\Delta\mu/kT]$, where $\Delta\mu$ is the chemical potential hindering the cooperative rearrangement per atom with $\Delta\mu > 0$. The cooperative transition probability is proportional to Ω and may be written $P(T) = A \exp[-z\Delta\mu/kT]$, where A is weakly temperature dependent and assumed constant in AGSC. The average transition probability $P_{av}(T)$ is determined by summing over all values of P(T), corresponding to different z at fixed temperature and pressure. If the assumption is made that the overwhelming majority of transitions take place in regions whose size differs negligibly from z^*, defined as the lower limit of the size of CRRs that have nonvanishing transition probabilities, then the average transition probability is:

$$P_{av}(T) = A \exp\left[\frac{-z^*\Delta\mu}{kT}\right]. \quad (11)$$

Expression 11 implies that the overwhelming number of transitions take place in regions having the smallest possible size, z^*. To complete the analysis, it is necessary to evaluate the temperature dependence of the z^*, the lower limit on CRR with nonzero transition probabilities. Arguments made by Adam and Gibbs (1965) enabled an estimate of z^* in terms of the molar

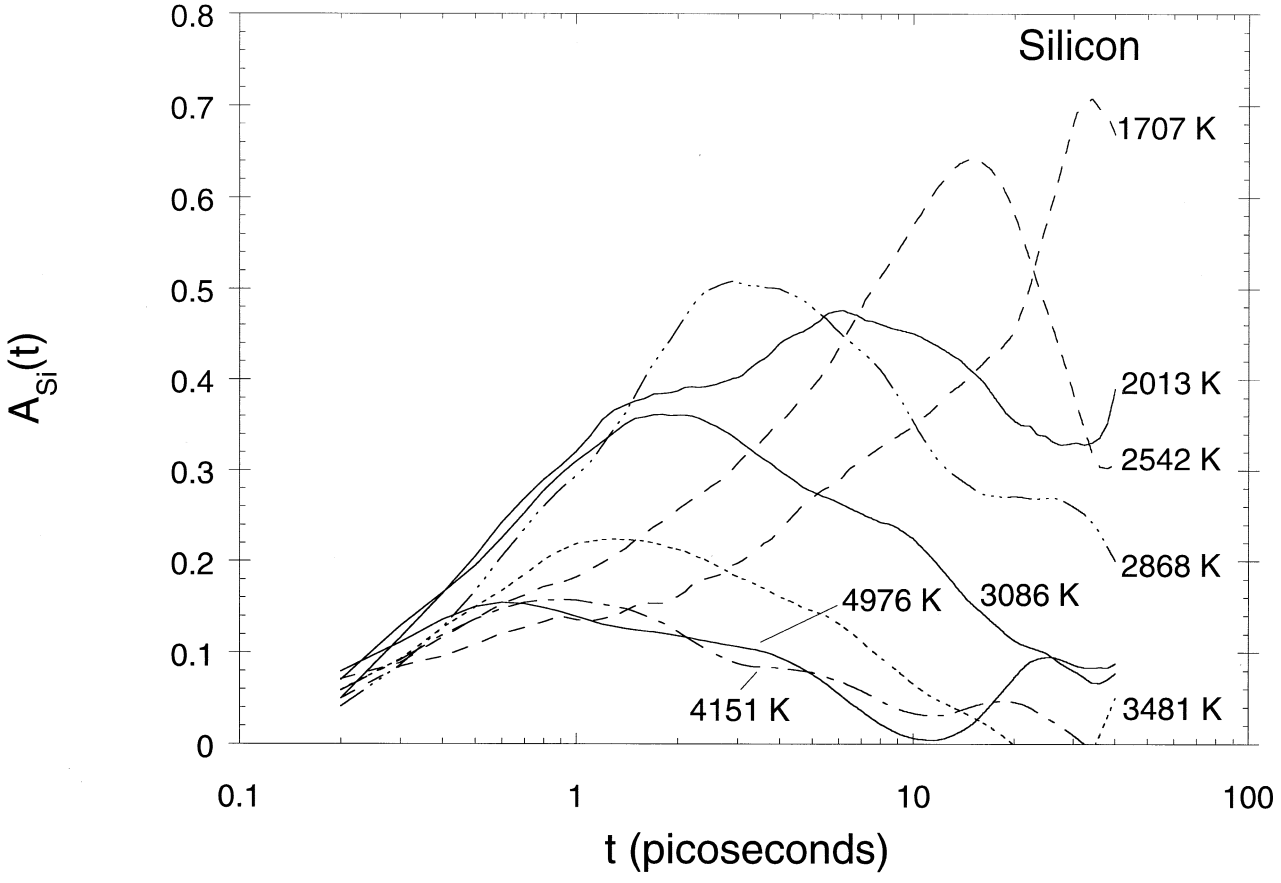

Fig. 11. Nongaussian parameter for silicon, $A_{Si}(t)$. See text for discussion.

configurational entropy S_{conf} of the macroscopic sample to be made. They posited that

$$z^* = \frac{N_A s_c^*}{S_{conf}} \tag{12}$$

where s_c^* is the critical configurational entropy of the minimum-sized CRR consisting of z^* atoms and N_A is Avogadro's number. By combining Eqns. 11 and 12 and assuming s_c^* to be constant, the average transition probability becomes

$$P_{av} = A\, exp\left[\frac{-B}{TS_{conf}(T)}\right] \tag{13}$$

where A and B are temperature-independent constants. Because the average transition probability is inversely proportional to the structural relaxation time and because the viscosity is directly proportional to the structural relaxation time, the shear viscosity assumes the form

$$\eta = A_e\, exp\left[\frac{B_e}{TS_{conf}(T)}\right] \tag{14}$$

where, again, A_e and B_e are temperature-independent constants.

By these rough statistical mechanical arguments, the relaxation characteristics of glass-forming liquids in AGSC are found to be related to macroscopic thermodynamic properties, notably the configurational entropy and its temperature derivative, the isobaric heat capacity. The dramatic increase in viscosity as T_g is approached is therefore related to the difference in entropy between (metastable) supercooled liquid and crystalline solid as temperature decreases in the deeply supercooled region. This difference arises solely as a result of configurational differences between supercooled liquid and its corresponding crystalline form. The entropy difference between supercooled liquid and crystalline solid decreases as temperature drops and is extrapolated to go to zero at a temperature called the Kauzmann temperature, T_K, where, in AGSC, a second-order thermodynamic transition is postulated to occur. The so-called Kauzmann paradox arises because extrapolation of the liquid and crystal entropy curves toward absolute zero leads to the disturbingly unphysical situation of negative entropy for supercooled liquid, a violation of the third law of thermodynamics. By allowing for a second-order thermodynamic phase transition at T_K, the paradox is sidestepped.

Calorimetric data for a number of silicate substances shows that the practical laboratory glass transition temperature (associated with a characteristic relaxation time of ~100 s) usually lies 30 to 50 K above T_K (Richet, 1984; Richet and Bottinga, 1995). In AGSC model, the small number of possible CRRs available to the system around the calorimetric glass transition is measured by the smallness of the molar configurational entropy (i.e., the difference in entropy of supercooled liquid

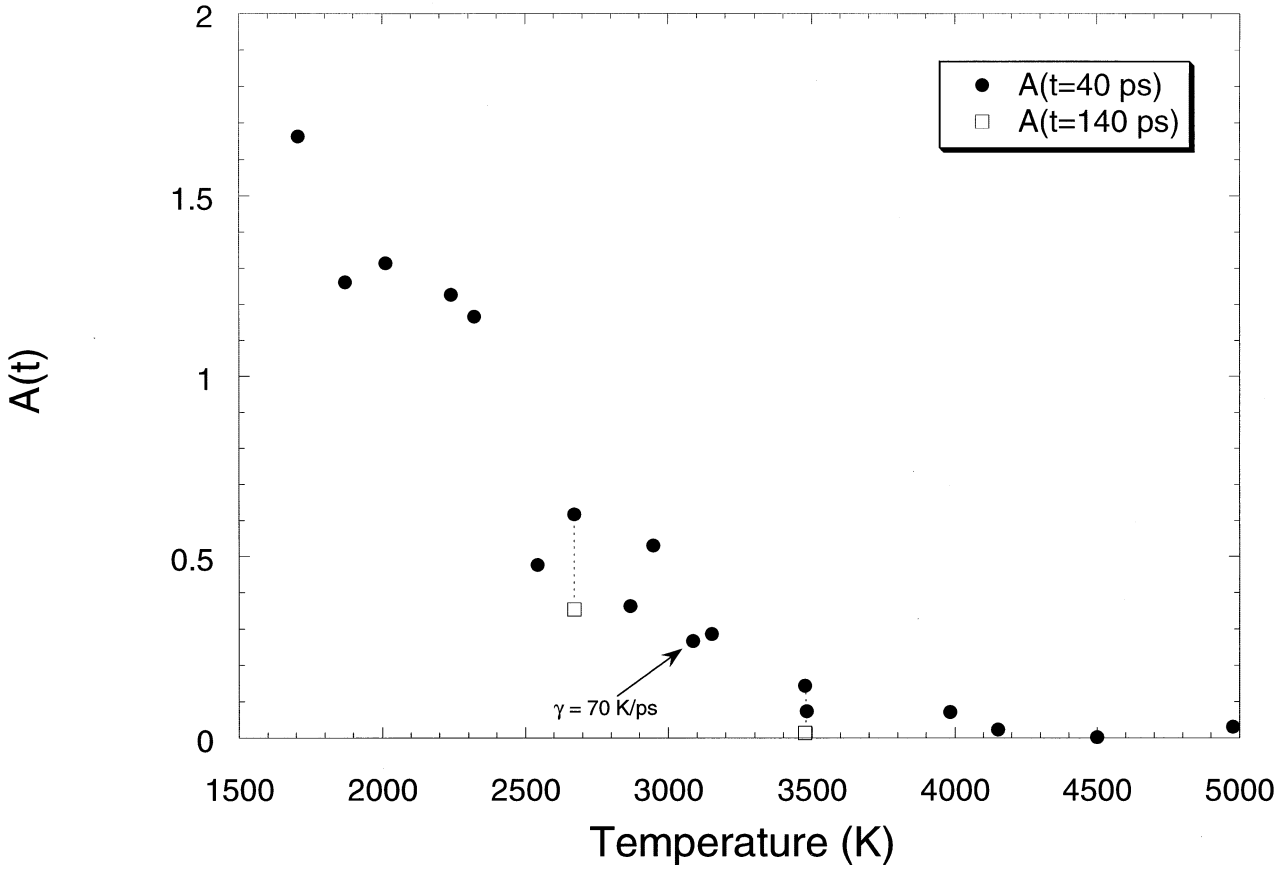

Fig. 12. Nongaussian parameter for oxygen vs. temperature at 40 ps (solid dots) and 140 ps (open squares). In the limit $t \to \infty$, $A_\alpha(t) \to 0$ for $T > T_g$, whereas $A_\alpha(t) \to$ a finite positive value at $T < T_g$.

and crystal) of supercooled liquid around T_g. At T_K, the extrapolated entropy goes to zero and the relaxation time and viscosity diverges. In terms of configuration space, the idea is that the system has fallen into a deep nondegenerate amorphous potential energy minimum at T_K, the temperature of an ideal glass transition. In practice, the kinetic glass transition intervenes before a supercooled liquid can be cooled to T_K.

Although AGSC theory is based on the idea of a CRR, the

Table 3. Best-fit parameters to the KWW expression, the hydrodynamic approximation to the relaxation time, t_H, the ratio t_o/t_H, and the slope obtained from the log-log plot of the MSD vs. time (as in Fig. 1), β_D.

T (K)	k_{min} (Å^{-1})	C	β_{KWW}	t_o (ps)	t_H (ps)	t_o/t_H	β_D
1707	0.23661	0.99993	0.19507	3.2025×10^{13}	22181	1.4438×10^{9}	0.17707
1871	0.23780	0.99743	0.79216	23050	7217.3	3.1937	0.31661
2013	0.23958	0.99773	0.60980	86822	5051.4	17.1877	0.35086
2239	0.23757	0.99614	0.83398	9006.6	3585.0	2.5123	0.37854
2320	0.23964	0.99665	0.92135	3377.3	2192.2	1.5406	0.49662
2542	0.23940	0.99743	0.67744	5600.0	1202.5	4.6570	0.55651
2670	0.23786	0.99706	0.81111	1647.9	1136.8	1.4496	0.68990
2868	0.23777	0.99963	0.72681	1227.6	571.49	2.1481	0.66516
2947	0.23607	0.99471	0.98502	482.2	441.61	1.0919	0.72774
3086	0.23662	1.0044	0.65611	1166.3	393.15	2.9666	0.70388
3150	0.23661	0.99747	0.92784	260.14	246.85	1.0538	0.80878
3475	0.23637	0.98631	0.99838	160.43	152.47	1.0522	0.90347
3481	0.23661	0.99862	0.91667	139.73	132.21	1.0569	0.86056
3983	0.23561	1.0012	0.95591	73.694	68.968	1.0685	0.94540
4151	0.23661	0.98297	1.10600	52.645	57.379	0.9175	0.92938
4500	0.23661	0.98643	1.08930	39.17	41.705	0.9392	0.94989
4976	0.23137	0.98314	1.08280	33.949	31.942	1.0628	0.96912

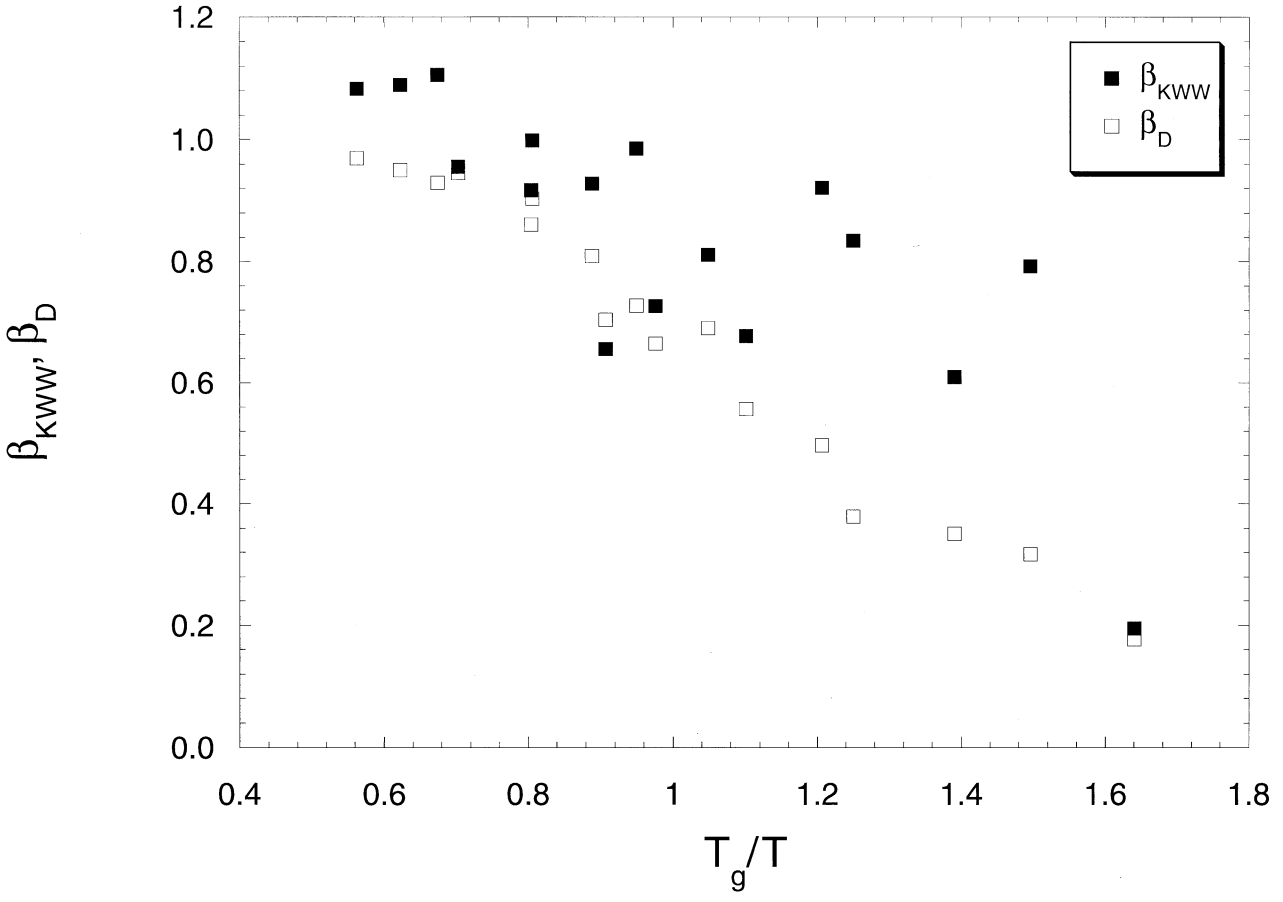

Fig. 13. Comparison of the stretched exponent power-law index β_{KWW} computed from fit of scattering function to KWW form (Eqn. 10 and Table 3) to the slope, β_D, obtained from a linear fit of the logarithm of the MSD vs. the logarithm of time for the simulations in Table 2.

theory itself does not provide a means for calculating the size of such a region until the excess entropy per atom of the minimum-sized CRR is specified. There is no way to determine this from the AGSC model self-consistently without making additional guesses. As an extreme limit, the entropy of the smallest region capable of undergoing a rearrangement is $s_c^* = k \ln 2$, because an absolute minimum of two complexions must be available for a rearrangement to take place. Adopting this value, $\Delta\mu$ and z^* may be calculated by means of experimental data. The value for the chemical potential so computed from laboratory calorimetric data is much larger than is physically plausible for $CaAl_2Si_2O_8$. In addition, the computed value of z^* is less than one, which is clearly devoid of physical meaning. Other examples of materials for which the AGSC theory breaks down are cited by Laughlin and Uhlmann (1972). This is not surprising in light of the approximations involved in deriving the theory. Although the AGSC hypothesis—especially the idea of the critical role played by cooperative motion—remains a powerful concept that serves the purpose of providing a connection between thermodynamic and viscometric properties, AGSC theory provides little quantitative insight into the microscopic dynamics of relaxation despite its statistical mechanical origin.

Despite its transparent inadequacies, AGSC theory does serve to approximately correlate calorimetric properties with transport properties for some liquids reasonably well. Richet (1984) and Richet and Bottinga (1995) have demonstrated that macroscopic viscosity–temperature data for liquid $CaAl_2Si_2O_8$ is consistent with the laboratory calorimetric data and AGSC predictions. The configurational entropy in Eqn. 14 is given by

$$S_{conf}(T) = S_{conf}(T_g) + \int_{T_g}^{T} \frac{\Delta C_{p\,conf}}{T} dT. \qquad (15)$$

The configurational entropy of glassy $CaAl_2Si_2O_8$ at T_g is identical its residual (0 K) entropy. The configurational isobaric heat capacity is closely approximated by the heat capacity difference between supercooled liquid and the harmonic solid Dulong and Petit limit of 3R/g-atom K. For a material such as silica with a nearly constant value of the configurational entropy (i.e., $\Delta C_p \approx 0$), an Arrhenian relation is recovered from Eqns. 14 and 15 because $S_{conf}(T) = S_{conf}(T_g)$ is a constant and Eqn. 14 reduces to the usual Arrhenian form with the identification $E_a = RB_e/S_{conf}(T_g)$. In contrast, melts with large changes in the isobaric heat capacity at T_g (such as $CaAl_2Si_2O_8$) exhibit significant curvature in log η − 1/T co-

ordinates. The vanishing of the extrapolated entropy difference at T_K is conceptually linked to the empirical Tamman-Vogel-Fulcher expression for the shear viscosity given by $\ln \eta \propto B/(T - T_o)$, where B and T_o are constants; evidently, the viscosity diverges asymptotically as $T \rightarrow T_o$. T_o may be identified with T_K, provided a hyperbolic expression for the temperature-dependent liquid heat capacity is assumed in computing the configurational entropy (i.e., $\Delta C_p \propto 1/T$). Although some silicate liquids, especially those rich in titania or ferric oxide (e.g., $Na_2TiSi_2O_5$), do exhibit $\Delta C_p \propto 1/T$ behavior (see Tangeman and Lange, 1998), this form is not universal. Molten $CaAl_2Si_2O_8$, $CaMgSi_2O_6$, $NaAlSi_3O_8$, and many natural compositions (e.g., rhyolite and dacite) exhibit linear behavior of ΔC_p vs. T. For especially strong network fluids such as SiO_2, the melt isobaric heat capacity is essentially constant.

In summary, the presence of a second-order thermodynamic phase transition underlying the glass transition is the essential idea of the AGSC hypothesis. The AGSC model is limited in that it provides no information on the size or number of CRRs because the configurational entropy of the critically sized CRR is not specified, except as a formal lower limit that provides, in practice, no useful insight at the microscopic level. A further problematic aspect of the theory is the validity of extrapolation of the supercooled liquid isobaric heat capacity in the temperature range $T_K < T < T_g$. That is, one cannot measure the configurational entropy of the supercooled liquid near T_K because the laboratory glass transition intervenes at $T = T_g > T_K$. Although the model demands knowledge of the heat capacity around T_K, this temperature interval is experimentally inaccessible, and one must be content with an extrapolation that cannot physically be tested.

4.3. STDM

Odagaki (1988) and Odagaki with coworkers (see also Odagaki and Hiwatari, 1990a,b, 1991; Hiwatari et al., 1991; Miyagawa et al., 1991; Odagaki et al., 1994) developed a hybrid thermodynamic–statistical model, STDM, for the glass transition. In STDM, the vibrational and hopping motions are separated and identified with the fast β relaxation and slow α relaxation, respectively. The motion associated with vibration in a local β basin in the $\mathbf{\Phi}$-scape is irrelevant with respect to transport properties around T_g. In contrast, the motion associated with the α relaxation (transitions between megabasins in the $\mathbf{\Phi}$-scape) is a nontrapped jump motion characterized by a waiting time distribution for the elementary cooperative relaxation process. In this view, the singular behavior of the ad hoc jump rate distribution function near zero jump rate is responsible for the glass transition. Below T_g, anomalous diffusion takes place such that as $t \rightarrow \infty$, MSD $\sim t^{\beta}$ with $\beta < 1$. The jump rate follows a power law with exponent λ, where λ is a thermodynamic dimensionless parameter related to the Kauzmann entropy crisis. The jump waiting time distribution determines the physical properties of the material during slow α relaxation. In particular, the diffusion constant is proportional to the reciprocal of the mean waiting time defined $< t_w > = \omega_o (\lambda + 1)/\lambda$, where ω_o is an "attempt" rate (vibration frequency) of a trapped (caged) atom in its local β basin. At high temperature, ω_o is of order 10^{-13} s^{-1}. In STDM, $\lambda = 0$ is identified as the glass transition. For $-1 < \lambda < 0$, $\beta = \lambda + 1$, whereas for $\lambda > 0$, $\beta = 1$. The parameter λ is the scaling parameter of the transition defined by Odagaki et al. (1997) in terms of the product of the excess (configurational) entropy and the temperature, the same product appearing in the AGSC theory. The order parameter in STDM is defined

$$\lambda = \frac{TS_{conf}(T) - T_g S_{conf}(T_g)}{T_g S_{conf}(T_g)}. \tag{16}$$

At $T = T_K$, the configurational entropy vanishes, $\lambda = -1$, and the jump waiting time distribution diverges according to $t^{-(\lambda+2)}$. Recall that a second-order phase transition takes place at $T = T_K$. The system displays nonergodic behavior because all of phase space cannot be explored, although relaxation still occurs in restricted portions of phase space sampled during the observation (or MD simulation) time. The glass transition in STDM represents the transition from gaussian to nongaussian atomic motion associated with the decay of microscopic density fluctuations. The nongaussian parameter in the long-time limit is taken as an order parameter of the transition. In STDM, the scattering function asymptotically decays toward zero for all temperatures, whereas the nongaussian parameter $A_\alpha(t)$ in the limit $t \rightarrow \infty$ and β begin to deviate from equilibrium liquid values of $A_\alpha(t = \infty) = 0$ and $\beta_D = 1$. Because the time required for the displacement associated with stochastic jump motion to become comparable to "cage drift" gets longer and longer as the glass transition is approached, so does the time t^* at which $A_\alpha(t)$ takes its maximum value $A^* = A(t^*)$. The product A^*t^* therefore shows a sharp decrease as the transition is approached from below. In Figure 14, $\log (A^*t^*)$ for Ca, O, Al, and Si is plotted vs. reciprocal temperature scaled by T_g. For T_g/T less than about unity, the relation $\log A^*t^* = a + b (T_g/T)$ holds for all atoms with b = 3.7 and 3.6 for O and Ca and 3.2 and 2.6 for Al and Si, respectively.

Further connections between the macroscopic (laboratory) properties of $CaAl_2Si_2O_8$ liquid and its underlying microscopic dynamics may be found by explicitly computing the order parameter λ defined by Eqn. 16. From laboratory measurements (Richet and Bottinga, 1984), for the residual third law of entropy of glassy $CaAl_2Si_2O_8$, $S(T_g) = 36.8 \pm 4$ J/mol K and isobaric heat capacity data for liquid anorthite, $C_p = 400.722 + 20.243 \cdot 10^{-3}T$ J/mol K; the order parameter λ can be calculated setting the computer glass transition temperature to 2800 K. Because the isobaric heat capacity of $CaAl_2Si_2O_8$ liquid is nearly constant at high temperature, the necessary extrapolation of laboratory data does not introduce appreciable error. An example based on the nongaussian characteristics of oxygen is shown in Figure 15. The macroscopic-order parameter of the transition $(\lambda + 1)$, which is based on laboratory thermodynamic data, is plotted vs. $\log [(A^*t^*)^{-1}]$, a quantity computed from the MD simulations. This quantity is a measure of the magnitude and timescale characterizing nonexponential relaxation. Note that the glass transition in $CaAl_2Si_2O_8$ at $\lambda = 0$ $(T = T_g)$ is identified with a break in slope.

In summary, STDM is a statistical model that links macroscopic thermodynamic information to a microscopic picture involving cooperative, thermally activated hopping of atoms. A limitation is the ad hoc nature of the waiting time distribution that ultimately relates the nonexponential decay of microscopic density fluctuations to the thermodynamic state through the

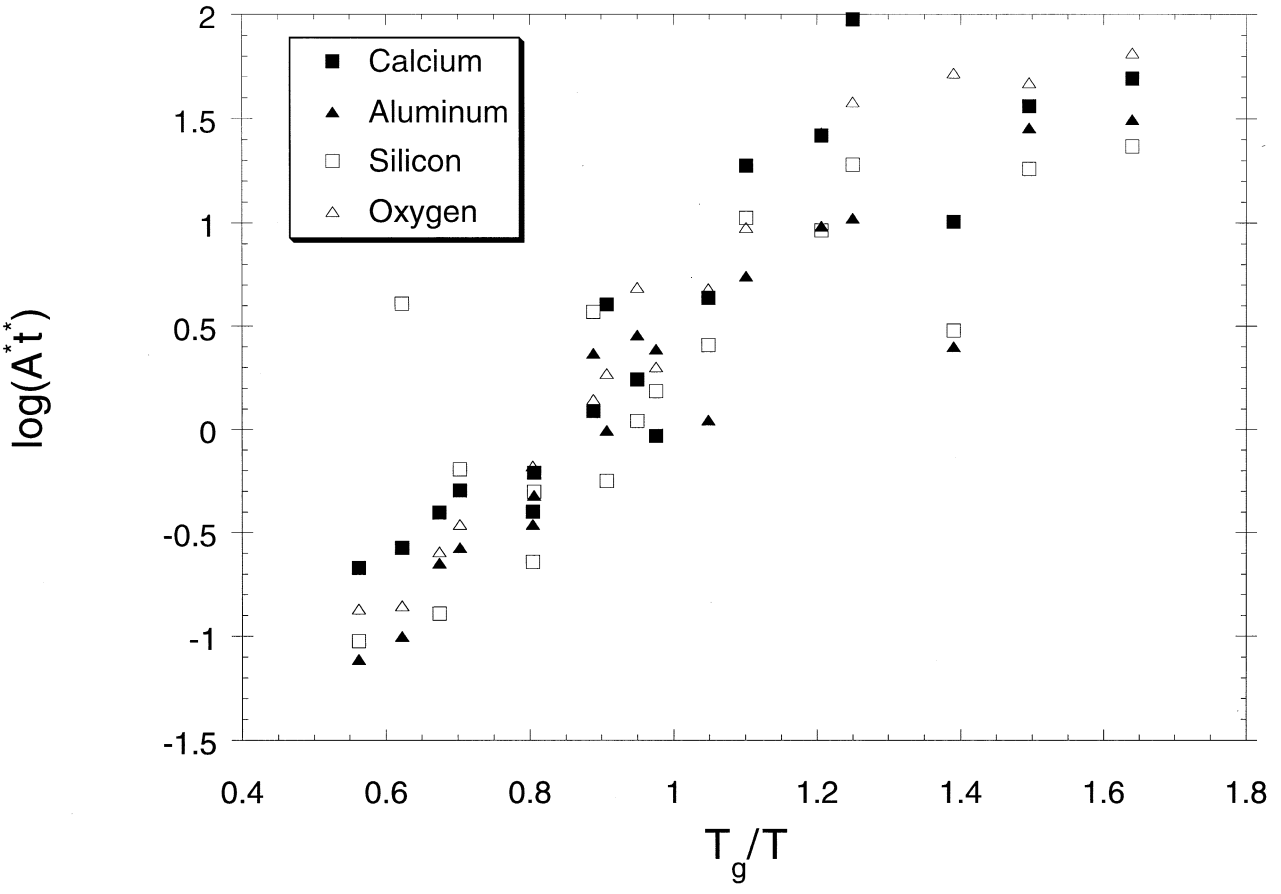

Fig. 14. Evidence of a gaussian to nongaussian transition for all species is noted in the logarithm of A^*t^* vs. T_g/T by sharp decrease in slope at approximately $T_g/T = 1$. For the high-temperature interval, $T_g/T < 1.2$, slopes of 3.7 and 3.6 for O and Ca. For Al and Si, the slopes are 3.2 and 2.6, respectively.

order parameter λ. The prediction MSD $\sim t^{\beta}$ of STDM only approximately holds. An appealing aspect is that nongaussinity in the decay of density fluctuations can be directly related to the waiting time distribution through thermodynamic scaling parameter λ.

4.4. Mode-Coupling Theories

Another theory of the glass transition is the MCT developed ~15 yr ago (Bengtzelius et al., 1984; Leutheusser, 1984; see also Debenedetti, 1996 for a review). MCT exploits the idea of a nonlinear feedback mechanism in which strongly coupled microscopic density fluctuations lead to structural arrest and diverging relaxation time at a critical temperature. In MCT, structural arrest arises solely from a positive feedback such that viscosity controls the shear relaxation time and hence viscosity itself (Geszti, 1983). That is, the relaxation time τ is decomposed into a vibrational and structural part ($\tau \approx \tau_{str} + \tau_{vib}$), and structural relaxation is explicitly related to tracer diffusion and hence the shear viscosity through the Einstein-Stokes relation. MCT is a strictly dynamic theory; no singularity in thermodynamic parameters is involved, as in AGSC and STDM. The idealized version of MCT (*i*MCT) posits a dynamic transition from ergodicity to nonergodicity at a critical temperature $T_c > T_g$, with viscosity exhibiting power-law divergence near T_c according to $D^{-1} \propto \eta \propto (T - T_c)^{-\gamma}$. Above T_c, where ergodicity is obeyed, all regions of phase space are accessible. Below T_c, where structural arrest occurs, parts of phase space remain inaccessible. A prediction of "ideal" MCT is that at $T < T_c$, the "self" part of the intermediate scattering function ($F_s(k,t)$) decays to a finite, nonzero number called the nonergodicity parameter in the limit $t \rightarrow \infty$. The nonergodicity parameter appears discontinuously at T_c. For $T > T_c$, *i*MCT predicts that the scattering function decays to zero in two steps. The first step is to a plateau (remaining there for some time), thereafter decaying to zero as $t \rightarrow \infty$. The time range in which the correlation function is close to the plateau is called the β relaxation regime and the regime that begins at the onset of deviation from the plateau is the α relaxation regime. For long times, the decay of the correlation function is approximated by the stretched exponential KWW function defined in Eqn. 10 above.

In the so-called extended version of MCT (*e*MCT), additional nonlinearities are accounted for in the differential equation for the time evolution of the scattering function. Retention of these terms has the effect of smearing out the transition region so that no divergence at T_c occurs. In *e*MCT, hopping

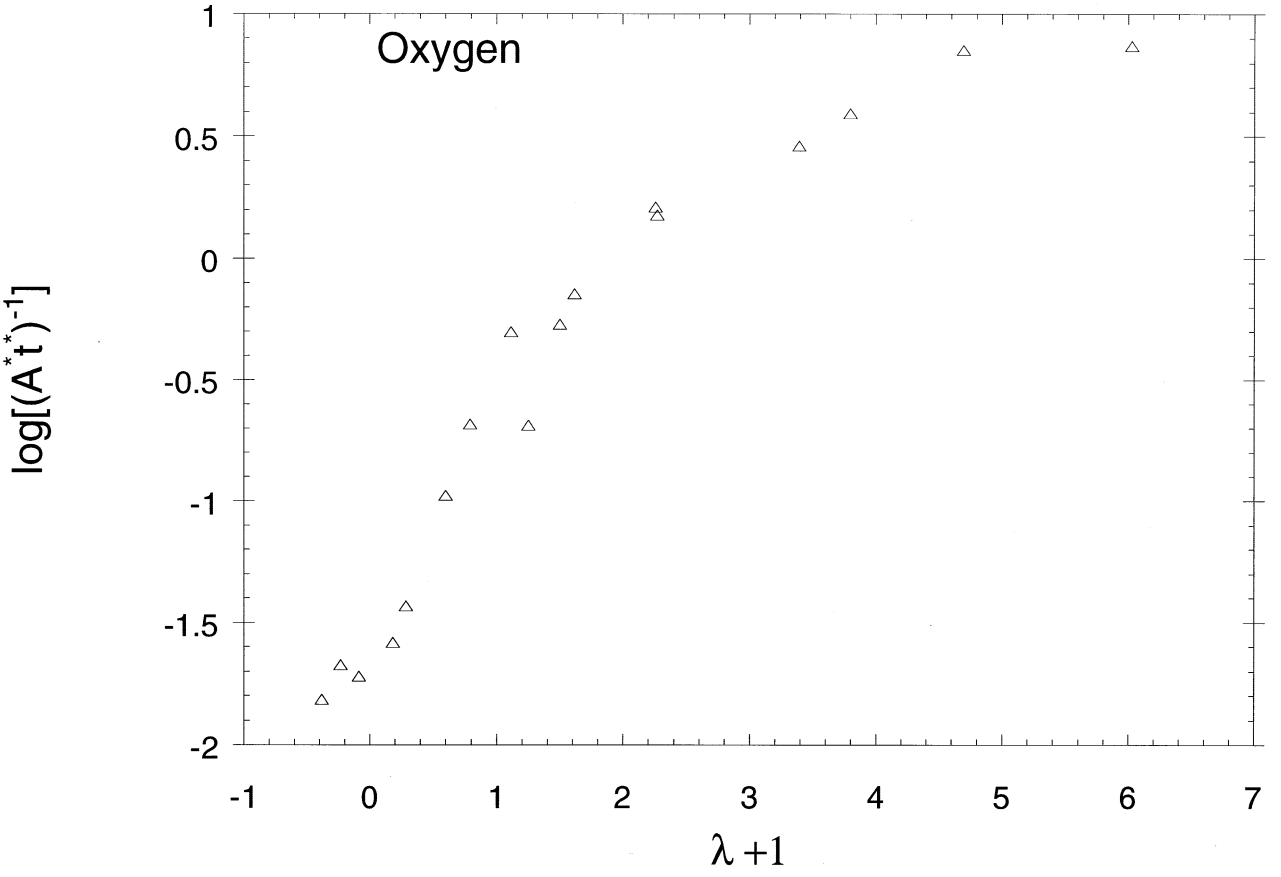

Fig. 15. Logarithm of inverse of A^*t^* for oxygen (purely a MD determined quantity) vs. $\lambda + 1$ (a laboratory-determined quantity), where λ is defined by Eqn. 16 with thermodynamic parameters defined in the text. Note that $\lambda = 0$ corresponds to the glass transition (T_g) of $CaAl_2Si_2O_8$.

motion is accounted for unlike *i*MCT where jump motion is neglected. As already noted from study of the van Hove correlation function (Figs. 2 to 5), hopping is indeed important in $CaAl_2Si_2O_8$. This is a clear limitation of *i*MCT in the description of thermally activated tracer diffusion in $CaAl_2Si_2O_8$.

In Figure 16, the tracer diffusivity of oxygen computed from the MD results is plotted vs. temperature. The solid curve is the best-fit Arrhenian curve to diffusivity data (Morgan and Spera, 2001) for $T > 3000$ K and the dashed curve is the fit to the MCT expression $D = A\,(T - T_c)^{\gamma}$. Computed fit parameters are: $\ln A = -30.830$, $T_c = 2593 \pm 125$ K and $\gamma = 1.53 \pm 0.14$. Although the MCT expression correlates the data slightly better than the Arrhenian fit, it may be argued that a three-parameter fit should perform better than a two-parameter (Arrhenian) fit. The value of the MCT critical temperature $T_c \approx 2600$ K is close to the computer glass transition estimate of T_g (≈ 2800 K), which is perplexing because one expects $T_c > T_g$ even for the high numerical quench rate of this MD study. For example, in the study of amorphous silica by Horbach and Kob (1999), the MCT critical temperature is $T_c \approx 3000$ K whereas the (computer) glass transition occurred at $T_g \approx 2850$ K. For amorphous $CaAl_2Si_2O_8$ the power-law exponent based on the MD data of $\gamma = 1.53$ is somewhat lower than the theoretical prediction of Sjörgen (1980) for hard spheres of $\gamma = 2.368$. On the basis of measured viscosity and taking $\eta \propto D^{-1}$, Angell (1988) reported values $1.5 < \gamma < 2.3$ for the power-law exponent for a number of liquids. The computed value for $CaAl_2Si_2O_8$ falls at the lower end of this range. For comparison, $\gamma = 2.05$ for silica as determined from MD simulations by Horbach et al. (1998) that use the potential of van Beest et al. (1990).

In summary, MCT describes some aspects of the relaxation dynamics of supercooled $CaAl_2Si_2O_8$ reasonably well, at least semiquantitatively, although T_c appears somewhat smaller than expected. In *e*MCT, the coupling between density and momentum fluctuations is included. These terms allow for thermally activated hopping at $T < T_c$, thereby restoring ergodicity to lower temperature, clearly an improvement upon *i*MCT. Detailed predictions of the *e*MCT theory remain to be worked out. Although T_c is clearly not the glass transition, it does appear to match the temperature at which significant nongaussian effects become important.

5. CONCLUSIONS AND FUTURE DIRECTIONS

Because MD quench rates are many orders of magnitude greater than laboratory rates, the computer glass transition temperature lies above the calorimetric one. This is true for a broad range of materials independent of the form of the interaction potential and is consistent with both the universality and

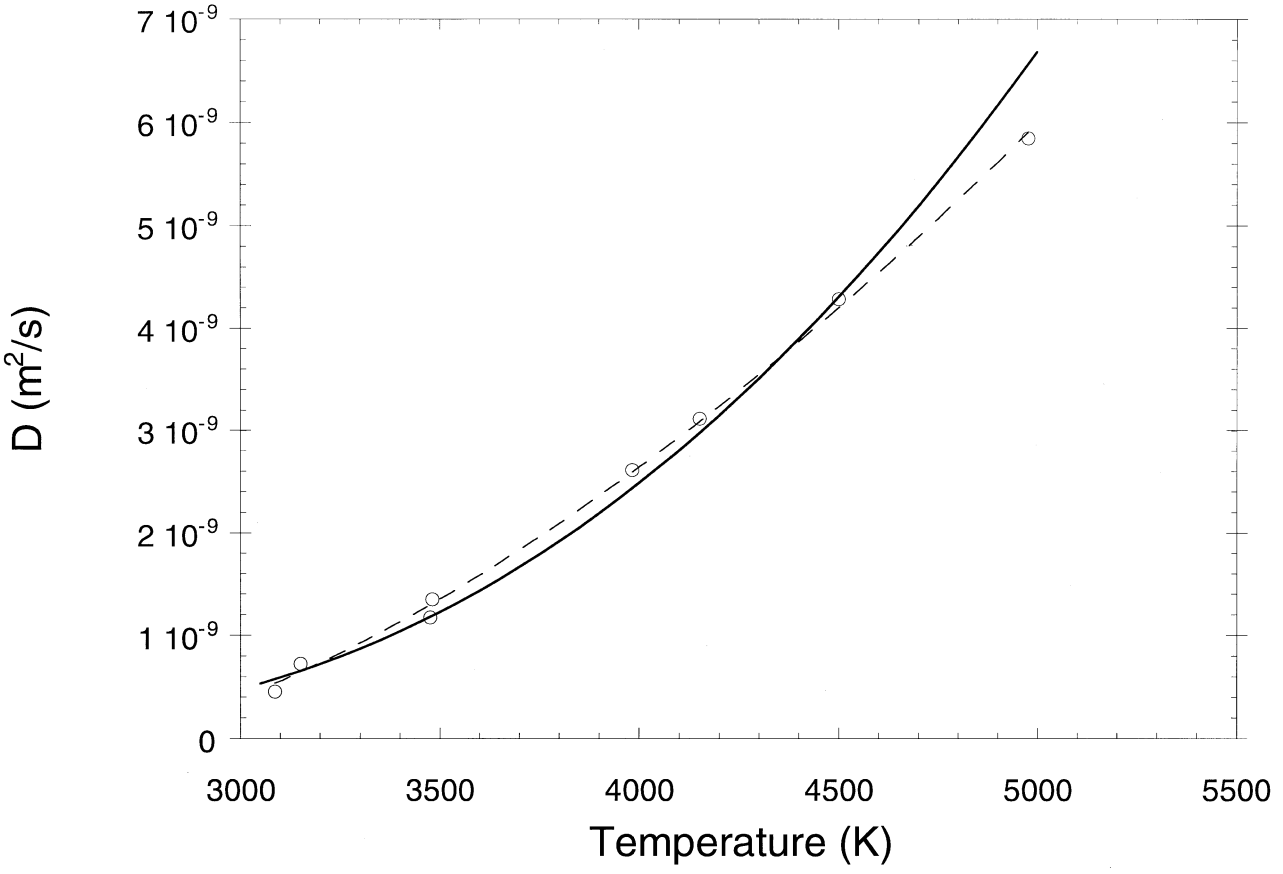

Fig. 16. Comparison of Arrhenian and MCT expressions for temperature dependence of oxygen tracer diffusivity. Solid curve is Arrhenian fit and dashed line is MCT fit to MD data for $T > 3000$ K (see text for details).

"kinetic" nature of the laboratory glass transition. T_g represents the temperature at which the structural relaxation time of the material is comparable to the timescale of experimental measurement. It appears that MD simulations provide a valid view of the glass transition, despite differences in the numerical values for the computer and laboratory glass transition temperatures.

The MD simulations provide clear evidence for the cooperative nature of thermally activated diffusion around the glass transition. The small range in computed tracer diffusivity at a given temperature and activation energy (170 to 190 kJ/mol) for Ca, O, Si, and Al is consistent with cooperative dynamics. The van Hove correlation functions reveal that oxygen and calcium diffuse by hopping between nearest self-neighbor sites at temperatures around T_g. Although not analyzed in detail, there appear to be correlations between epochs of nongaussian behavior in the decay of microscopic density fluctuations between all atoms, but especially oxygen and calcium, for example. The mechanism of coupling between oxygen and Ca involves the accessibility of jump sites controlled by relaxation of the O-Si-Al network. The intermediate scattering function exhibits stretched exponential behavior that is a reflection of the distribution of atom waiting times at individual sites. When this diffusion process is studied at a coarser scale, it leads to MSD $\sim t^{\beta}$ with $\beta < 1$ (i.e., subdiffusion). At a given temperature, the decay of the self-intermediate scattering function goes to the hydrodynamic limit more rapidly the smaller the magnitude of the wave vector. For a larger wave vector, the rate of decay of $F_s(k,t)$ becomes less exponential as higher moments become important. This indicates that on a short-length scale, motion of the atoms is nonrandom. This is especially marked for Ca and O. The nongaussian component of the decay of the intermediate scattering function, $A_\alpha(t)$, exhibits increasingly complex behavior as the temperature falls toward T_g from above. All atoms exhibit this same qualitative behavior around T_g.

Although each of the models for the glass transition explored provides some insight into the glass transition, no single model is consistent with all of the MD results. In AGSC, a second-order phase transition is postulated to occur at the Kauzmann temperature, $T_K < T_g$, where the entropy of supercooled liquid equals to the entropy of crystalline solid. In AGSC, the configurational entropy of metastable liquid goes to zero at T_K, and the resultant material is called an ideal glass. In this view, there is nothing fundamental about T_g. If a supercooled liquid could be cooled sufficiently slowly, T_K could be attained before intervention of the laboratory glass transition. Although the AGSC model enables one to estimate shear viscosity from calorimetric data (sometimes accurately), it provides little quantitative insight into the microscopic dynamics of the transition itself. STDM goes beyond AGSC in that it specifically relates relaxation dynamics to a physical picture—one of the

stochastic jump motion of a trapped atom from a caged site by cooperative motion of its neighbors, which are themselves caged. In STDM, the idea of a second-order thermodynamic transition at T_K is retained by definition of an order parameter of the transition. This order parameter, based on configurational entropy, is explicitly related to the waiting time distribution of caged particles. A power-law relationship is assumed such that at T_K the mean particle residence time diverges. MCT, on the other hand, is a purely dynamic theory that captures the non-exponential decay of density fluctuations in terms of a transition from ergodic to nonergodic behavior. It also specifies a power-law dependence of viscosity and tracer diffusivity on temperature that is consistent with the MD simulations at $T > T_g$.

The great promise of MD simulation is that when sufficiently large particle number and sufficiently long duration simulations are performed, constraints for a truly microscopic theory of the transition will emerge. For a simple Lennard-Jones fluid, this approach has already proven enlightening (e.g., Poole et al., 1998; Donati et al., 1999; Doliwa and Heuer, 1999; Kegel and van Blaaderen, 2000; Ediger, 2000; Weeks et al., 2000). These studies, taken collectively, suggest that relaxation occurs through the motion of groups (mesoscale?) of relatively few, cooperatively moving atoms that cluster or organize spatially in three-dimensional (Euclidean) space. These CRRs may relax independently from each other at different rates leading to non-Debye relaxation. The precise relationship between this "dynamic heterogeneity" and the CRR remains unclear. Detailed studies have not yet been extended to multicomponent silicate melts of geochemical importance, although it is anticipated that such studies will be completed in the future.

Acknowledgments—This research was supported by the U.S. Department of Energy BES-Geoscience program and the National Science Foundation-EAR division. The comments of three anonymous reviewers and associate editor Dr. C. Romano greatly improved the presentation of this work.

Associate editor: C. Romano

REFERENCES

Adam G. and Gibbs J. H. (1965) On the temperature dependence of cooperative relaxation properties in glass-forming liquids. *J. Chem. Phys.* **43,** 139–146.

Allen M. P. and Tildesley D. J. (1987) *Computer Simulation of Liquids.* Oxford University Press.

Angell C. A. (1988) Perspectives on the glass transition. *J. Phys. Chem.* **49,** 863–871.

Angell C. A. (1991) Relaxation in liquids, polymers and plastic crystals—Strong/fragile patterns and problems. *J. Non-Crystal. Solids* **131,** 13–31.

Angell C. A., Ngai K. L., Kieffer J., Egami T., and Nienhaus G. U., eds. (1997) *Structures and Dynamics of Glasses and Glass Formers.*Materials Research Society Symposium Proceedings.

Bengtzelius U. Götze W., and Sjölander A. (1984) Dynamics of supercooled liquids and the glass transition. *J. Phys. C* **17,** 5915–5934.

Binder K., ed. (1995) *Monte Carlo and Molecular Dynamics Simulations in Polymer Science.* Oxford University Press.

Bottinga Y. (1994) Configurational entropy and the non-Newtonian rheology of homogeneous silicate melts. *Phys. Rev. B* **49,** 95–99.

Bottinga Y., Richet P., and Sipp A. (1995) Viscosity regimes of homogeneous silicate melts. *Am. Mineral.* **80,** 305–318.

Bryce J. G., Spera F. J., and Stein D. J. (1999) Pressure dependence of self-diffusion in the $NaAlO_2$-SiO_2 system: Compositional effects and mechanisms. *Am. Mineral.* **84,** 345–356.

Debenedetti P. G. (1996) *Metastable Liquids: Concepts and Principles.* Princeton University Press.

Doliwa B. and Heuer A. (1999) The origin of anomalous diffusion and non-Gaussian effects for hard spheres: Analysis of three-time correlations. *J. Phys. Condensed Matter* **11,** A277–A283.

Donati C., Glotzer S. C., and Poole P. H. (1999) Growing spatial correlations of particle displacements in a simulated liquid on cooling toward the glass transition. *Phys. Rev. Lett.* **82,** 5064–5067.

Ediger M. D. (1996) Supercooled liquids and glasses. *J. Phys. Chem.* **100,** 13200–13212.

Ediger M. D. (2000) Movies of the glass transition. *Science* **287,** 604–605.

Fredrickson G. H. (1988) Recent developments in dynamical theories of the liquid–glass transition. *Ann. Rev. Phys. Chem.* **39,** 149–180.

Geszti T. (1983) Pre-vitrification by viscosity feedback. *J. Phys. C* **16,** 5805–5814.

Gibbs J. H. (1956) Nature of the glass transition in polymers. *J. Chem. Phys.* **25,** 185–195.

Gibbs J. H. and DiMarzio E. A. (1958) Nature of the glass transition and the glassy state. *J. Chem. Phys.* **28,** 373–383.

Goldstein M. (1969) Viscous liquids and the glass transition: A potential energy barrier picture. *J. Chem. Phys.* **51,** 3728–3739.

Goldstein M. (1976) Viscous liquids and the glass transition. V. Sources of the excess specific heat of the liquid. *J. Chem. Phys.* **64,** 4767–4774.

Hansen J. P. and McDonald I. R. (1986) *Theory of Simple Liquids.* Academic Press.

Hiwatari Y., Miyagawa H., and Odagaki T. (1991) Dynamical singularities near the liquid–glass transition: Theory and molecular dynamics study. *Solid State Ionics* **47,** 179–222.

Horbach J., Kob W., and Binder K. (1998) Molecular dynamics simulation of the dynamics of supercooled silica. *Phil. Mag. B* **77,** 297–303.

Horbach J. and Kob W. (1999) Static and dynamic properties of a viscous silica melt. *Phys. Rev. B* **60,** 3169–3181.

Kauzmann W. (1948) The nature of the glassy state and the behavior of liquids at low temperatures. *Chem. Rev.* **43,** 219–256.

Kegel W. K. and van Blaaderen A. (2000) Direct observation of dynamical heterogeneities in colloidal hard-sphere suspensions. *Science* **287,** 290–293.

Kob W. (1995) Computer simulations of supercooled liquids and structural glasses. *Ann. Rev. Comp. Phys.* **3,** 1–43.

Kob W. (1999) Computer simulations of supercooled liquids and glasses. *J. Phys. Condensed Matter* **11,** R85–R115.

Laughlin W. T. and Uhlmann D. R. (1972) Viscous flow in simple organic liquids. *J. Chem. Phys.* **76,** 2317–2325.

Lesher C. E., Hervig R. L., and Tinker D. (1996) Self diffusion of network formers (silicon and oxygen) in naturally occurring basaltic liquid. *Geochim. Cosmochim. Acta* **60,** 405–413.

Leutheusser E. (1984) Dynamical model of the liquid–glass transition. *Phys. Rev. A* **29,** 2765–2773.

Miyagawa H., Hiwatari Y., and Itoh S. (1991) Molecular-dynamics study for the glass transition in LiI. *Progr. Theor. Phys.* **103,** 47–60.

Morgan N. A. and Spera F. J. (2001) A molecular dynamics study of the glass transition in $CaAl_2Si_2O_8$: Thermodynamics and tracer diffusion. *Am. Mineral.*, **86,** 915–926.

Nevins D. and Spera F. J. (1998) Molecular dynamics simulations of molten $CaAl_2Si_2O_8$: Dependence of structure and properties on pressure. *Am. Mineral.* **83,** 1220–1230.

Odagaki T. (1988) Anomalous and subanomalous diffusion in stochastic trapping transport. *Phys. Rev. B.* **38,** 9044–9053.

Odagaki T. and Hiwatari Y. (1990a) Stochastic model for the glass transition of simple classical liquids. *Phys. Rev. A.* **41,** 929–937.

Odagaki T. and Hiwatari Y. (1990b) Stochastic model for a glass transition. *J. Non-Crystal. Solids* **117/118,** 887–889.

Odagaki T. and Hiwatari Y. (1991) Gaussian–to–non-Gaussian transition in supercooled fluids. *Phys. Rev. A.* **43,** 1103–1106.

Odagaki T., Matsui J., and Hiwatari Y. (1994) Trapping diffusion model for glass transition and slow dynamics in supercooled liquids. *Physics A* **204,** 464–481.

Odagaki T., Matsui J., Fujisaki M., Higuchi M. (1997) A unified theory

for the glass transition dynamics and its singularities. In *Structures and Dynamics of Glasses and Glass Formers* (eds. C. A. Angell, K. L. Ngai, J. Kieffer, T. Egami, and G. U. Nienhaus), 455, pp. 163–169. Materials Research Society Symposium Proceedings.

Pakula T. and Teichmann J. (1997) A model for relaxation in supercooled liquids and polymer melts. In *Structures and Dynamics of Glasses and Glass Formers* (eds. C. A. Angell, K. L. Ngai, J. Kieffer, T. Egami, and G. U. Nienhaus), 455, pp. 211–222. Materials Research Society Symposium Proceedings.

Poole P. H., Donati C., and Glotzer S. C. (1998) Spatial correlations of particle displacements in a glass-forming liquid. *Physics A* **261,** 51–59.

Rahman A., Singwi K. S., and Sjölander A. (1962) Theory of slow neutron scattering by liquids. *J. Phys. Rev.* **126,** 986–996.

Richet P. (1984) Viscosity and configurational entropy of silicate melts. *Geochim. Cosmochim. Acta* **48,** 471–483.

Richet P. and Bottinga Y. (1984) Anorthite, andesine, wollastonite, diopside, cordierite and pyrope: Thermodynamics of melting, glass transitions, and properties of the amorphous phases. *Earth Planet. Sci. Lett.* **67,** 415–432.

Richet P. and Bottinga Y. (1995) Rheology and configurational entropy of silicate melts. In *Structure, Dynamics and Properties of Silicate Melts* (eds. J. F. Stebbins, P. F. McMillan, and D. B. Dingwell), **32,** pp. 67–93. Mineralogical Society of America.

Rustad J. R., Yuen D. A., and Spera F. J. (1990) Molecular dynamics of liquid SiO_2 under high pressure. *Phys. Rev. A.* **42,** 2081–2089.

Scamehorn C. A. and Angell C. A. (1991) Viscosity–temperature relations and structure in fully polymerized aluminosilicate melts from ion dynamics simulations. *Geochim. Cosmochim. Acta* **55,** 721–730.

Sjörgen L. (1980) Numerical results on the velocity correlation function in liquid argon and rubidium. *J. Phys. C.* **13,** 705–715.

Stebbins J. F., McMillan P. F., and Dingwell D. B., eds. (1995) *Structure, Dynamics, and Properties of Silicate Melts.* Mineralogical Society of America.

Stein D. J. and Spera F. J. (1995) Molecular dynamics simulations of liquids and glasses in the system $NaAlSiO_4$-SiO_2: I: Methodology and melt structures. *Am. Mineral.* **80,** 417–431.

Stein D. J. and Spera F. J. (1996) Molecular dynamics simulations of liquids and glasses in the system $NaAlSiO_4$-SiO_2; physical properties and transport mechanisms. *Am. Mineral.* **81,** 284–302.

Stillinger F. H. (1995) A topographic view of supercooled liquids and glass formation. *Science* **267,** 1935–1939.

Tangeman J. A. and Lange R. A. (1998) The effect of $Al^{3+}$and Ti^{4+}on the configurational heat capacities of sodium silicate liquids. *Phys. Chem. Mineral.* **26,** 83–89.

van Beest B. W. H., Kramer G. J., and van Santen R. A. (1990) Force fields for silicates and aluminophosphates based on *ab initio* calculations. *Phys. Rev. Lett.* **64,** 1955–1958.

Weeks E. R., Crocker J. C., Levitt A. C., Schofield A., and Weitz D. A. (2000) Three-dimensional direct imaging of structural relaxation near the colloidal glass transition. *Science* **287,** 627–631.

Zallen R. (1983) *The Physics of Amorphous Solids*. Wiley-Interscience.

Zarzycki J. (1991) *Glasses and the Vitreous State*. Cambridge University Press.